

Zuni–Bandera volcanism, Rio Grande, USA — Melt formation in garnet- and spinel-facies mantle straddling the asthenosphere–lithosphere boundary

Timothy J. Peters^{a,*}, Martin Menzies^a, Matthew Thirlwall^a, Philip R. Kyle^b

^a Department of Geology, Royal Holloway University of London, Egham, Surrey, TW20 OEX, England, United Kingdom

^b N.M. Bureau of Geology and Mineral Resource, N.M. Institute of Mining and Technology, Socorro, N.M. 87801, USA

Received 17 October 2006; accepted 6 August 2007

Available online 16 August 2007

Abstract

The Zuni–Bandera Volcanic Field (ZBVF) is a late-Neogene volcanic field on the boundary of the stable Colorado Plateau and the active Rio Grande Rift. Alkalic and tholeiitic magmas have erupted through Proterozoic continental crust with the tholeiitic magmas having undergone shallow-level fractional crystallization of olivine±clinopyroxene±spinel. The alkaline–tholeiitic lava flows lack elemental and isotopic correlations usually indicative of concomitant crust assimilation and fractional crystallization (AFC) and appear to have inherited their geochemistry from sub-Moho depths. Consideration of isotopic data, and modelling of REE and U–Th data constrains the mantle-melting history. The tholeiite basalts are primarily spinel-facies mantle melts (95–100% for spinel-facies), whereas the alkali basalts have a much higher proportion of garnet-facies mantle melts (15–25% for all samples except QBO 607 assumed to be 100% garnet-facies). The increased contribution from garnet-facies mantle in the alkali basalts is supported by U–Th isotopic data, where a shift towards ²³⁰Th excess is observed. Since the lithospheric thickness increases from 45–55 km beneath the Rio Grande Rift, to 120–150 km beneath the Colorado Plateau, the ZBVF volcanic rocks are most likely a mixture of asthenosphere-derived (garnet-facies) alkali basalts and lithosphere-derived (spinel-facies) tholeiitic basalts. This is further supported by Sr–Nd isotopic data with alkali basalts having isotopic compositions similar to depleted-mantle values (⁸⁷Sr/⁸⁶Sr=0.702986 to 0.70378, ¹⁴³Nd/¹⁴⁴Nd=0.512712 to 0.512978), while the tholeiite basalts have higher ⁸⁷Sr/⁸⁶Sr (0.704725 to 0.706003) and lower ¹⁴³Nd/¹⁴⁴Nd (0.512379 to 0.512913) typical of basaltic magmas derived from ancient, LREE-enriched lithospheric mantle. Overall, melting is observed to be polybaric in nature, with mixing of melts over an extended depth range with the development of melting columns that span (a) the garnet-to spinel-facies phase boundaries in the mantle, and, (b) the asthenosphere–lithosphere boundary.

© 2007 Elsevier B.V. All rights reserved.

Keywords: Garnet facies; Spinel facies; Rio Grande rift; Colorado plateau; Zuni–Bandera; Rare Earth Elements

1. Introduction

Late Cenozoic lithospheric extension in western North America was accompanied by considerable intra-plate basaltic magmatism, (e.g. Leeman, 1982; Ormerod et al., 1988; Fitton et al., 1991; Baldrige et al., 1991;

* Corresponding author. Department of Earth and Environmental Sciences, Vanderbilt University, VU Station B #351805, 2301 Vanderbilt Place, Nashville, TN 37235-1805, USA. Tel.: +1 615 322 2976; fax: +1 615 322 2138.

E-mail address: Timothy.J.Peters@Vanderbilt.edu (T.J. Peters).

Wang et al., 2002). During extension, decompression of the mantle leads to development of melt columns (Klein and Langmuir, 1987) where normal potential temperature (1300 °C) convecting sub-lithospheric mantle begins to replace thinned lithosphere. With advanced lithospheric extension, decompression of the continental lithosphere and input of heat from upwelling asthenosphere begins to change the thermal state of the lower lithosphere, increasing its potential to generate magma (e.g. Fitton et al., 1991). Mafic volcanism in the Rio Grande Rift is observed to have sources first in the lithosphere (McMillan, 1998; McMillan et al., 2000), where the physical properties at the base of the lithosphere are changed to that of the warm ductile asthenosphere while maintaining its chemical properties (Perry et al., 1987, 1988). Eventually, with evolving geothermal gradients and/or the physical removal of the lithosphere due to thermal erosion by upwelling asthenosphere (Perry et al., 1987, 1988) and the increasingly refractory nature of the lithosphere with progressive melting and removal of volatile components emplaced during metasomatic events (McMillan, 1998; McMillan et al., 2000), the lithosphere becomes an exhausted reservoir for melt generation and the asthenospheric mantle begins to dominate as a source for continental volcanism (McMillan, 1998; McMillan

et al., 2000). Consideration of the lithospheric and asthenospheric contributions during the genesis of volcanic fields throughout the western USA has produced an insight into the regional distribution and nature of mantle domains partially melted during extension. In general, relative elemental concentrations and isotopic data from such volcanic rocks have been correlated with geophysical parameters (i.e. crustal and lithospheric thickness, xenolith thermobarometry, surface heat flow), to quantify the extent of mantle domains beneath the western USA (Menzies et al., 1983; Perry et al., 1987, 1988; Lum et al., 1989; Menzies, 1989; Menzies and Kyle, 1990; Menzies et al., 1991; Kempton et al., 1991; Wang et al., 2002; Thompson et al., 2005).

Late-Neogene extension on the western flank of the Rio Grande rift (Baldrige et al., 1991), and production of the Jemez lineament by crustal shearing and rotation of the Colorado Plateau, as discussed by Spence and Gross (1990), were associated with the eruption of the Zuni–Bandera volcanic field (ZBVF) (Fig. 1), a region of mixed basanite, alkali basalt, and tholeiite lava flows. Menzies and Kyle (1990) and Menzies et al. (1991) proposed a model where by the chemistry of the ZBVF magmas was explained by the interaction of three mantle sources (i.e. asthenosphere, lower lithosphere, and a mantle plume). The consequence of this model was that basanites were

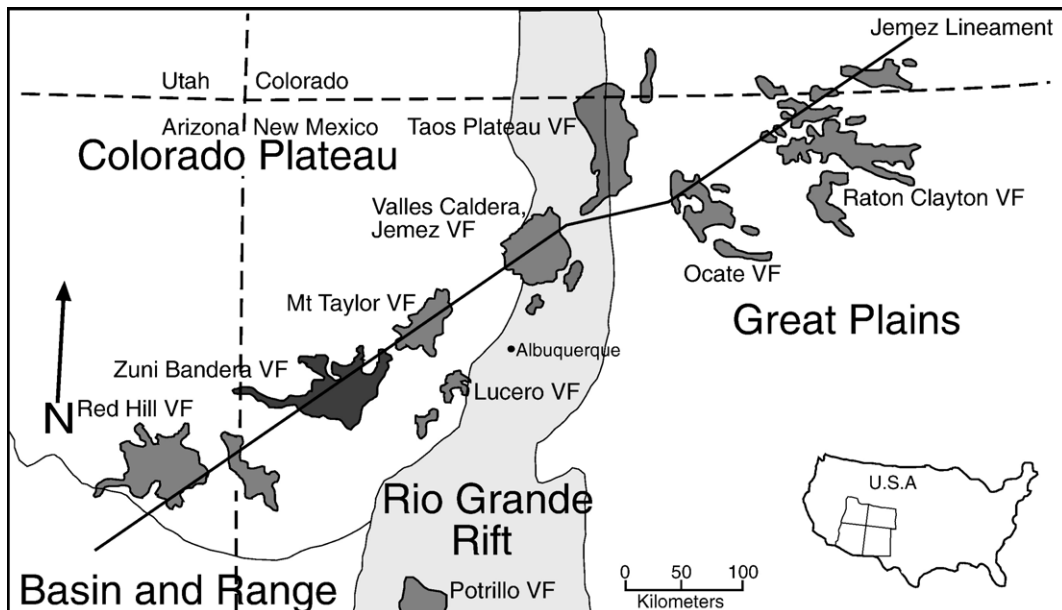


Fig. 1. General tectonic and volcanic map of Northern New Mexico, USA. Tectonic features include the extensional Rio Grande rift and Basin and Range, and stable lithospheric regions of the Great Plains and Colorado Plateau. Volcanic fields (VF) can be observed to lie along with the Jemez lineament. The Zuni Bandera Volcanic Field resides on the western flank of the Rio Grand rift in a transitional region with the Colorado Plateau. After Goff and Grigsby (1982).

believed to have originated within the convecting asthenospheric mantle ($^{87}\text{Sr}/^{86}\text{Sr}$ ratio < 0.703), whereas the tholeiitic basalts were extracted from the lithospheric mantle or a plume-contaminated asthenospheric mantle ($^{87}\text{Sr}/^{86}\text{Sr}$ ratio > 0.706).

The objective of this paper is to address several issues relating to the petrogenesis of the ZBVF magmas and to unravel their polybaric melting history. To constrain the extent and depth of partial melting along with the mantle facies involved in melt production, we will use elemental and Sr–Nd isotopic data, U–Th disequilibria data, and variations in rare earth element (REE) solid: melt partitioning.

2. Geological setting

Located in west central New Mexico (Fig. 1), the ZBVF comprises a sequence of mixed tholeiite and alkali basalt lava flows, spatter ramparts, scoria cones, small shields, maars, and collapse pits erupted through Proterozoic continental crust over the last 1.5 Ma (Anders et al., 1981; Maxwell, 1986; Baldrige et al., 1991; Menzies et al., 1991). The ZBVF is located in the transitional zone between the actively extending terrains of the Rio Grande rift and the Basin and Range province, and the relatively stable southern edge of the Colorado Plateau (Fig. 1). Across this region the asthenosphere–lithosphere boundary varies significantly in depth from 45–55 km beneath the Rio Grande rift, to 120–150 km beneath the Colorado Plateau (West et al., 2004).

Over the past 4.5 Ma, volcanism in the environs of the Rio Grande rift has been to some degree decentralised from the rift to the Jemez Lineament (Fig. 1), an 800 km NE-trending crustal discontinuity that cuts across the rift. This decentralization is defined by the spatial distribution of late-Cenozoic volcanic fields, including the Zuni–Bandera Volcanic Field (Spence and Gross, 1990). Seismic tomography has identified regions of low P-wave velocities beneath the Jemez Lineament, interpreted as evidence of the presence of melt, and may suggest that the lineament acts as a conduit for magma transport beneath these volcanic fields (Spence and Gross, 1990; Menzies et al., 1991). Interestingly, recent teleseismic studies by West et al. (2004) across the Rio Grande rift revealed the absence of a deep-mantle low-velocity anomaly beneath the region of extension. This supports the interpretation of lithospheric extension and magmatism as results of stresses localised within the lithosphere and small-scale mantle convection, rather than deep-mantle upwelling due to the presence of an active plume/thermal anomaly beneath the rift (West et al., 2004).

3. Analytical techniques

3.1. Major and trace elements

Major and trace element data were produced for ca 33 samples from ZBVF lava flows. Data were acquired at RHUL using a Philips PW1480 X-ray fluorescence spectrometer (XRF) and techniques summarized by Thirlwall et al. (1997). Trace elements were determined on pressed pellets and major elements on fused glass discs. During fused glass disc preparation, crushed rock samples were initially heated to 1100 °C for 30 min to oxidize FeO to Fe₂O₃, producing a sample weight change or loss on ignition (LOI). The ignited sample was then reweighed and flux powder added in a 1 part sample 6 parts flux ratio, as to avoid issues of LOI sample weight changes. The results are displayed in Table 1. Data for the standard BHVO1 (as an example) and analytical reproducibility (± 2 S.D.) are included in Table 1.

3.2. REE and U–Th data

REE concentrations and U–Th data were determined for selected samples first analysed by Menzies et al. (1991) with additional Sr–Nd isotopic ratios produced for samples that lacked such data in their original study. REE and U–Th data were determined using isotope dilution analysis at RHUL. Powdered samples were spiked with a Th–U spike, a mixed LREE spike (La, Ce, Nd, Sm, Eu, and Gd), and a mixed HREE spike (Dy, Er, Yb, and Lu) (Thirlwall, 1982). The isotopic spikes are calibrated relative to the same gravimetric mixed REE standard solution as used by Thirlwall (1982). The standard analyses reported therein are relevant to samples analyzed for this study. Analysis involved a Micromass IsoProbe Multi-Collector Inductively coupled plasma mass spectrometer (MC-ICP-MS), using a Cetac Aridus desolvating nebulizer.

The standard “Table Mountain Latite” (TML) was used during analyses of U–Th data. Standard isotopic values of TML, from Seth et al. (2003), are as follows: ($^{230}\text{Th}/^{238}\text{U}$) = 1.0010 ± 10 (2 S.D., $n=5$); ($^{230}\text{Th}/^{232}\text{Th}$) = 1.0766 ± 80 (2 S.D., $n=8$). The precision (2 S.E.) for the measured REE (ppm) and U–Th concentrations (ppb) expressed as % of concentration are as follows: Nd < 0.25%; Sm < 0.07%; Eu < 0.02%; Ce < 2.23%; La < 1.678%; Gd < 0.45%; Dy < 0.10%; Er < 0.02%; Yb < 0.04%; Lu < 0.02%; Th < 569.5% to 7.65%; U < 18.47% to 1.65%.

3.3. Sr–Nd isotopes

Sr and Nd were separated from digested samples using standard ion-exchange techniques. Sr samples were

Table 1
Major (wt.%) and trace element (ppm) geochemistry of the ZBVF lavas

	±2 S.D.	MJ89 001	MJ89 006	MJ89 007	MJ89 008	MJ89 011	MJ89 014	MJ89 016	MJ89 017	MJ89 018	MJ89 037	MJ89 043
Unit		Qb	Qb	Qc	Qb	Qc	W	W	W	W	Qv	Qc
Lat. °N		34°37'30''	34°47' 45''	34°47' 56''	34°47' 19''	34°45'17''	34°43' 14''	34°41' 53''	34°43' 22''	34°43' 25''	34°49' 07''	34°47'34''
Long. °W		108°22'22''	108°16' 22''	108°16' 55''	108°16' 12''	108°18' 12''	108°21' 41''	108°21' 33''	108°20' 37	108°20' 35''	108°14' 34''	108°14' 45''
Location		Cerro de las Mujeres	Cerro Alto	Cerro Alto	Cerro Alto	Laguna Colorado					Cerro Chato	Cerro Colorado
Basalt type		Tholeiite	Tholeiite	Tholeiite	Tholeiite	Tholeiite	Tholeiite	Tholeiite	Tholeiite	Tholeiite	Tholeiite	Tholeiite
SiO ₂	0.3	51.04	55.11	52.67	53.93	56.93	47.69	50.66	56.96	57.12	51.12	46.26
TiO ₂	0.01	1.262	1.577	1.772	1.553	1.352	1.805	1.371	1.233	1.229	1.477	2.337
Al ₂ O ₃	0.1	14.95	15.11	15.56	14.57	15.52	14.32	15.26	15.38	15.49	16.06	14.59
Fe ₂ O ₃	0.05	11.45	8.88	9.82	8.96	8.83	12.43	11.57	8.9	8.7	11.13	12.17
MnO	0.01	0.166	0.137	0.151	0.143	0.134	0.172	0.162	0.131	0.129	0.155	0.177
MgO	0.1	8.97	6.09	6.46	7.86	4.47	9.49	8.16	4.74	4.85	6.74	9.9
CaO	0.05	9.28	7.29	7.87	7.36	6.23	9.09	9.58	6.39	6.48	9.57	9.24
Na ₂ O	0.1	2.51	3.45	3.34	3.45	3.53	3.43	2.56	3.37	3.4	2.68	2.84
K ₂ O	0.004	0.434	1.897	1.71	1.845	2.279	0.949	0.455	2.146	2.25	0.796	1.434
P ₂ O ₅	0.01	0.141	0.335	0.38	0.345	0.263	0.34	0.162	0.356	0.234	0.231	0.541
Total		100.21	99.86	99.72	100.02	99.54	99.71	99.94	99.6	99.88	99.95	99.49
Sc	0.8	24	19	21	19	17	24	21	16	16	22	25
V	1.5	163	158	179	161	131	180	147	114	124	168	221
Cr	1.5	270	210	218	299	91	265	216	118	115	101	306
Ni	1	217	103	102	174	72	216	150	87	85	95	205
Cu	1.5	96	42	45	45	56	105	86	45	60	72	55
Zn	1	93	72	83	75	82	103	83	72	74	79	101
Ga	0.9	19	18.5	17.6	16.5	19.4	19.4	18	18.7	18	18.5	20.5
Rb	0.5	11.2	28	25.3	26.3	38.1	8.5	10	35.9	36	11.1	17.1
Sr	2	222	542	577	531	339	243	251	315	312	333	878
Y	0.6	19	21.5	22.8	21	23.2	21.4	18.4	20.6	21.4	20.2	25.2
Zr	1	82	188	199	187	181	95	87	168	167	121	239
Nb	0.5	6.5	28.4	31.1	28.4	27.9	9.2	7.8	24.7	25.3	13.7	43
Ba	5	100	522	463	478	350	102	108	363	352	218	344
La	2	7	29	27	30	28	10	10	27	28	14	31
Ce	2	19	50	52	48	52	22	18	49	52	30	66
Nd	1	10	22	24	21	22	12	10	20	21	15	31
Pb	0.5	2.3	7.7	7.3	7.4	9	1.1	2.2	8.4	8.2	3.3	4.1
Th	0.4	1.7	3.3	3.6	3.1	6.1	0	1.4	4.8	4.6	2.1	3.8

Data for the standard BHVO1 (as an example) and analytical reproducibility (± 2 S.D.) are included. Geological units correspond to those from Maxwell (1986).

loaded onto single Ta beads and Nd samples loaded onto single Re beads with phosphoric acid and silica gel. $^{143}\text{Nd}/^{144}\text{Nd}$ and $^{87}\text{Sr}/^{86}\text{Sr}$ ratios were determined using a VG354 5-collector Thermal Ionisation Mass spectrometer at RHUL using the procedures described by Thirlwall (1991a,b). Results are given in Table 2. The SRM 987 international standard was used for Sr and an in-house Aldrich standard for Nd. Analysis of standards during 2004–2006 are as follows: SRM987 gave $^{87}\text{Sr}/^{86}\text{Sr} = 0.710250 \pm 14$ (2 S.D., $N=269$); Aldrich gave $^{143}\text{Nd}/^{144}\text{Nd} = 0.511404 \pm 6$ (2 S.D., $N=52$). The slightly lower values for Aldrich relative to that reported by Thirlwall

(1991b) reflects preparation of fresh standard solutions; the previous solution had small amounts of Pr and appears to have been slightly contaminated by Nd.

4. Results

4.1. Chemical classification

The ZBVF samples mostly have less than 51.5 wt.% SiO₂, with a few samples at higher silica contents (i.e. >52% SiO₂). Using the TAS diagram of Le Bas et al. (1986) (Fig. 2) the ZBVF samples are classified as

MJ89 044	MJ89 048	MJ89 056	MJ89 071	MJ89 073	MJ89 123	MJ89 140	MJ89 146	MJ89 155	MJ89 158	MJ89 061	MJ89 077	MJ89 078
Qc	Qv	Qbu	Qc	Qb		Qbt	Qbc	Qbm	Qbm	Qc	Qcb	Qvb
34°47'05''	34°47' 58''	34°51' 02''	34°57' 05''	34°56' 14''	35°16' 25''	34°59' 00	35°05' 24''	35°03' 42''	34°47' 05''	34°45' 33''	35°59' 54''	35°00' 09''
108°14' 56''	108°14' 09''	108°13' 58''	108°09' 42''	108°08' 15''	107°39' 23''	108°01'	107°47'	107°42' 30''	107°56' 32''	108°10' 50''	108°05'	108°04' 26''
Cerro Colorado	Cerro Chato	Cerro Piedrita	Cerro Comadre	Cerro Rendija	Mt. Taylor	Twin Crater	El Calderon	McCarty Flow	McCarty Flow	Cerro Brillianto	Bandera Crater	Bandera Crater
Tholeiite	Tholeiite	Tholeiite	Tholeiite	Tholeiite	Tholeiite	Tholeiite	Tholeiite	Tholeiite	Tholeiite	Alkali	Alkali	Alkali
46.61	47.72	50.63	48.67	51.82	47.85	49.32	50.7	50.68	51.56	43.2	46.83	44.59
2.369	2.165	1.633	1.822	1.546	2.054	1.447	1.427	1.4	1.37	3.018	2.17	2.827
14.73	14.66	17.01	14.63	15.59	15.19	14.89	14.45	14.82	15.39	12.01	15.02	14.77
12.17	11.44	10.86	12.26	11.46	11.73	12.23	12.09	11.91	11.48	12.63	11.6	13.62
0.169	0.174	0.161	0.175	0.159	0.161	0.176	0.167	0.16	0.16	0.196	0.18	0.176
10.16	10.36	6.41	9.03	6.09	8.04	9.31	8.63	7.86	7.9	10.6	9.49	8.9
8.94	9.32	9.55	9.13	9.83	8.39	8.92	8.87	9.04	9.34	10.61	9.2	8.85
3.13	3.13	2.89	2.91	2.82	4	2.85	2.74	2.7	2.63	3.6	3.69	3.82
1.519	1.441	0.775	0.915	0.526	1.679	0.722	0.722	0.69	0.69	2.069	1.574	1.65
0.56	0.421	0.276	0.317	0.221	0.678	0.23	0.199	0.19	0.19	1.073	0.543	0.589
100.35	100.82	100.19	99.86	100.06	99.78	100.1	100	99.5	100.75	99.01	100.3	99.79
25	25	21	27	25	20	23	24	26	25	24	25	20
229	221	188	200	194	176	172	175	179	174	244	205	218
295	365	58	280	86	213	256	280	260	250	332	287	127
208	211	63	197	100	140	197	206	168	160	209	173	138
54	61	66	82	95	40	81	103	95	101	53	47	55
95	85	81	98	98	110	92	99	101	95	111	88	108
19.5	18.4	18	18.5	19.5	22.1	18.5	18.9	18.3	18	18.5	18.6	21.2
19	15.4	9.8	12.5	7.6	26.7	13.8	16.3	15.2	14	49.5	18.8	18.5
659	592	396	401	294	842	304	279	274	279	1126	693	744
25	22.7	21.8	24	22.6	23.5	23	24.5	24.2	22.8	33.7	24.4	22.1
244	202	141	155	111	237	122	121	121	117	361	220	252
44.1	33	18	19.6	9.9	48.2	13.3	10.1	9.8	10.1	90.3	39.2	42.5
419	305	341	216	162	790	171	174	170	164	886	349	338
31	25	18	16	10	38	12	12	13	12	74	32	34
69	54	36	40	25	74	29	25	31	27	146	68	71
32	26	18	20	14	36	15	16	15	14	66	30	34
5.3	4.3	3.7	3.8	2.8	5.5	3.1	3.8	4.6	3.7	6.4	4.1	3
4.1	3.3	2	2.7	1	5.3	2.2	2.4	2	2.2	10.2	4	3.4

(continued on next page)

basanite (10); trachybasalt or hawaiite (3); basalt (14); and basaltic andesite (6). In the following discussion the samples have been sub-divided into tholeiite basalts (Hy-normative) and alkali basalts (Ne-normative).

4.2. MgO versus major elements

MgO contents in the ZBVF lava flows vary from 4.5 to 10.6 wt.%, with the lowest values generally coupled with the highest SiO₂ contents. MgO-variation diagrams (Fig. 3) show that K₂O, SiO₂, and Al₂O₃ systematically increase with decreasing MgO, whereas CaO and MnO (not shown)

systematically decrease with decreasing MgO. Alkali basalts display a higher degree of enrichment in incompatible major elements (e.g. P₂O₅ and Na₂O) with steeper negative trends relative to tholeiite basalts. Fe₂O₃ variations between the suites contrast, with tholeiite basalts recording a positive correlation with MgO, and the alkali basalts show a general negative correlation. Non-systematic variations in TiO₂ with MgO are observed in both suites, although the alkali basalts have higher mean TiO₂ contents (>2 wt.%). The alkali basalt suite and the mafic members of the tholeiite suite (samples with <52 wt.% SiO₂) display trends typical of intraplate-type continental-rift basalts erupted

Table 1 (continued)

	MJ89 104	MJ89 105	MJ89 107	MJ89 108	MJ89 109	MJ89 112	MJ89 114	MJ89 116	MJ89 142	BHVO1 Measured	BHVO1 Recommended	BHVO1 2se
Unit	Qbp	Qbp	Qbo	Qbo	Qcp	Qbp	Qbz	Qbp	Qbb	Standard	Standard	Standard
Lat.°N	35°02' 14''	35°02' 13''	35°02' 16''	35°02' 35''	35°03' 38''	35°05' 04''	35°08'	35°07' 50''	34°59' 15''			
Long.°W	108°03' 51''	108°03' 54''	108°06' 31''	108°04' 37''	108°03' 39''	108°03' 19''	108°03' 03''	107°58' 58''	108°05' 45''			
Location	Paxton Springs	Paxton Springs	Oso Ridge	Oso Ridge	Paxton Springs	Paxton Springs	Cerro Colorado	Paxton Springs	Bandera Flow			
Basalt type	Alkali	Alkali	Alkali	Alkali	Alkali	Alkali	Alkali	Alkali	Alkali			
SiO ₂	44.26	46.26	44.71	45.83	44.64	44.74	45.3	45.02	46.12	50.04	49.9	0.067
TiO ₂	2.904	2.531	2.908	2.469	2.877	2.845	2.365	2.418	2.276	2.74	2.69	0.012
Al ₂ O ₃	14.2	15.66	15.2	15.51	14.35	14.77	14.35	14.57	14.81	13.76	13.85	0.039
Fe ₂ O ₃	13.38	14.06	14.23	13.82	13.48	13.64	11.93	12.51	12.24	12.27	12.23	0.018
MnO	0.186	0.163	0.169	0.162	0.184	0.18	0.179	0.18	0.179	0.171	0.17	0.004
MgO	9.41	5.42	6.25	5.54	9.38	8.82	10.09	10.07	10.08	7.32	7.31	0.04
CaO	9.03	7.34	7.91	7.32	8.97	8.83	9.18	9.56	9.29	11.38	11.33	0.038
Na ₂ O	3.68	5.99	4.9	5.21	3.57	3.6	3.89	3.15	3.18	2.31	2.29	0.049
K ₂ O	1.752	2.513	2.171	2.426	1.756	1.63	1.912	1.469	1.396	0.524	0.54	0.003
P ₂ O ₅	0.628	0.934	0.947	0.909	0.625	0.58	0.702	0.516	0.494	0.275	0.28	0.005
Total	99.43	100.87	99.39	99.19	99.84	99.63	99.9	99.46	100.06	100.79	0	100.59
Sc	20	9	10	11	22	22	22	27	27	31.8	31.8	1.1
V	232	147	178	152	251	232	206	237	225	314.4	317	2.5
Cr	204	61	59	65	225	228	292	241	268	281.7	289	2.6
Ni	154	68	75	76	171	155	167	167	198	117.5	121	1
Cu	55	35	40	38	55	52	43	54	57	135.8	136	0.8
Zn	98	178	154	172	107	92	87	84	94	99.9	105	0.6
Ga	19.8	27.7	25	27.1	21.3	19.4	19.9	18.5	18.3	20.7	21	1.1
Rb	20.6	29.5	25.1	28.5	21.1	18.6	19.9	17.2	16.5	9.5	9.1	0.4
Sr	783	1250	1210	1265	798	745	812	623	651	382.8	396.9	0.8
Y	23.4	19.8	21.1	19.9	24.4	23.1	22.6	24.2	24.3	26.5	27.6	0.4
Zr	279	366	350	356	289	260	275	212	205	179.3	180	1
Nb	47.6	62.7	65.1	61.9	49.6	44.6	49.7	34.9	35.2	19.1	19.8	0.3
Ba	360	505	521	492	345	315	370	289	324	138	135	3
La	35	70	59	72	49	32	37	27	27	16.7	15.6	2.1
Ce	75	142	126	145	76	70	78	62	61	38	39	3
Nd	38	63	57	64	36	33	36	28	29	23.2	24.9	1.3
Pb	4.8	4.9	4.4	4.4	2.9	4.4	4.8	3.3	5.1	3.2	2	0.7
Th	4.4	6.2	6.8	5.4	3.7	3.7	3.4	3.1	3.6	1.4	1.3	0.7

across the Rio Grande rift (e.g. Perry et al., 1987), at the Potrillo Volcanic field (PVF) in the southern Rio Grande rift (Thompson et al., 2005), in the Jemez Mountains on the Jemez lineament (Wolff et al., 2005), and across the Basin and Range (Wang et al., 2002).

4.3. Trace element chemistry

Magnesium variation diagrams (Fig. 4) display positive linear trends with Ni, Cr, and Sc for alkaline and tholeiitic rocks. The alkali basalts display negative correlations of La, Sr, Rb, and Zr with MgO, whereas the tholeiite basalts display less-steep to insignificant variations, a characteristic shared by other incompatible elements: i.e. LILE, Nb,

LREE, Th, and Na₂O. Pb concentrations increase with decreasing MgO wt.% for the tholeiite basalts, with a scattered near-horizontal trend in the alkali basalts.

The relative concentration of trace elements for the ZBVF lavas can be observed on primitive-mantle-normalized diagrams (Sun and McDonough, 1989) (Fig. 5a and b) where the two suites show similar patterns, but with some important differences. The tholeiite basalts display variable enrichments in Th, Ba, and Pb, with isolated samples containing depletions in Sr, Nb, and K, relative to the main trend of the suite. The alkali basalts show higher concentrations of all elements with specific depletions in Th, K, Pb, and enrichments in Sr and Ba. The steeper transition between Zr and Y, the depletions in Pb,

and the enrichments in La and Ce, displayed by the alkali basalts are similar to the normalized pattern for an ocean island basalt from Gough (Sun and McDonough, 1989).

4.4. Rare Earth Elements (REE) chemistry

Chondrite-normalised (Nakamura, 1974) REE plots for ZBVF lava flows (Fig. 5c) indicate a high level of compositional variability in light REE (LREE) and heavy REE (HREE) enrichment relative to chondrite (i.e. La = ~30 to 200 times chondrite). An important feature of the REE profiles is the variation in LREE/HREE ratios, with the alkali basalts showing the greatest variation and the tholeiite basalts showing slight flattening in the HREE (Er–Yb–Lu) profiles. Alkali basalt QBO 607 shows significant LREE enrichment and HREE depletion distinct from the other samples.

4.5. Sr–Nd isotope chemistry

The ZBVF continental intraplate volcanic rocks have a range in $^{87}\text{Sr}/^{86}\text{Sr}$ = 0.703625 to 0.706003 and $^{143}\text{Nd}/^{144}\text{Nd}$ = 0.512589 to 0.512891 (Table 2; Fig. 6). This compares well to the ZBVF range reported by Menzies et al. (1991: $^{87}\text{Sr}/^{86}\text{Sr}$ = 0.70299 to 0.70555 and $^{143}\text{Nd}/^{144}\text{Nd}$ = 0.51238 to 0.51297). The alkali basalts display the lowest $^{87}\text{Sr}/^{86}\text{Sr}$ and highest $^{143}\text{Nd}/^{144}\text{Nd}$ ratios, in the direction of modern normal mid ocean ridge basalts. The tholeiite basalts show elevated $^{87}\text{Sr}/^{86}\text{Sr}$ ratios above the Bulk Earth value and reduced $^{143}\text{Nd}/^{144}\text{Nd}$ ratios straddling the Bulk Earth value. These enriched isotopic ratios are more akin to those observed in enriched mantle sourced ocean island basalts, e.g. Pitcairn hotspot basalts ($^{87}\text{Sr}/^{86}\text{Sr}$ < 0.70529) (Eisele et al., 2002). The isotopic ratios observed in the ZBVF covers the range observed in basalts from the western USA (e.g. Leeman, 1982; Kempton et al., 1991) and the Rio Grande rift (e.g. Perry et al., 1987, 1988), with depleted values similar to alkali basalts from the Potrillo Volcanic field ($^{87}\text{Sr}/^{86}\text{Sr}$ < 0.70313) (Thompson et al., 2005) located on thinned lithosphere in the rift axis, and enriched values similar to basalts from the Jemez Mountains ($^{87}\text{Sr}/^{86}\text{Sr}$ 0.7040 to 0.7053) (Wolff et al., 2005) on the Jemez lineament.

5. Modification of the ZBVF primary magma composition

5.1. Fractional crystallization

The ZBVF lava flows show a range in MgO values between 4.47–10.60 wt.% and are coupled with significant

variations in Ni (39–251 ppm) and Cr (11–365 ppm), suggesting the possible influence of fractional crystallization on their primitive magma composition. Positive correlations between specific trace element concentrations and MgO wt.% (Fig. 4) suggest that the parental magmas for the ZBVF tholeiite and alkali basalts have undergone shallow fractionation of olivine (Ni) ± clinopyroxene (Sc) ± Cr-spinel (Cr). Decreases of MgO with CaO (Fig. 3), CaO/Al₂O₃ (not shown), Sc (Fig. 4), and V (not shown) indicate clinopyroxene fractionation to have been important in both suites; increases in Al₂O₃ and Sr with decreasing MgO (Figs. 3 and 4) indicate fractionation of a mineral assemblage without abundant plagioclase. Linear correlations between major elements and MgO wt.% (Fig. 3) coincide with fractional crystallization vectors and indicate the dominance of olivine + clinopyroxene as a fractionation assemblage. In general the tholeiitic and alkaline basalts do not appear to be related by the same fractionation process, which would produce a sequence of parallel or sub-parallel chondrite-normalised trace element patterns for elements incompatible with the shallow level fractionation assemblage.

Least-squares modelling of fractional crystallization was performed on data from Table 1 using the XLFRAC programme of Stomer and Nicholls (1978). A shallow level fractionation assemblage of olivine, clinopyroxene, and spinel was chosen based on the observations from magnesium variation diagrams (Fig. 4). Although most models produced poor results, the better models (where the sum of the square of the residuals, R² values, for trends produced by the programme are < 1) supported fractionation of olivine and clinopyroxene. The tholeiite basalts generally display < 10% olivine and < 10% clinopyroxene fractional crystallization, increasing to < 15% clinopyroxene with < 10% olivine fractionation for the alkali basalts.

Basaltic andesite samples with SiO₂ wt.% > 52 contain no evidence of a more extensive fractionation assemblage, that would explain their elevated silica contents. They share chemical similarities (K₂O > 1.5%, SiO₂ > 52%, low SiO₂/Rb ratio < 2, and low Sc/Rb ratio < 1) with volcanic rocks from the Taos Plateau Volcanic Field (Fig. 1; McMillian and Dungan, 1986). McMillian and Dungan (1986) explain such chemical features as the result of complex differentiation paths involving fractional crystallization, assimilation of crustal material, mafic recharge, and magma mixing. This complex path may explain similar samples in the ZBVF. However, the limited number of samples with > 52 wt.% SiO₂ and the lack of isotopic data, makes it difficult to evaluate this model.

Table 2
Major element (wt.%) geochemistry of the ZBVF lavas from Menzies et al. (1991)

	QBW201	QBW203	QBT302	QV101	QV906	QB203	QBJ402	QBM502	QBM801
Location	Hoya di Cibola	Hoya di Cibola	Twin Crater	Cinder Field	Cinder Field	Older Basalts	El Calderon	McCartys	McCartys
Basalt type	Tholeiite	Tholeiite	Tholeiite	Tholeiite	Tholeiite	Tholeiite	Tholeiite	Tholeiite	Tholeiite
SiO ₂	52.64	51.50	49.74	51.76	48.01	51.09	50.73	52.55	51.17
TiO ₂	1.32	1.21	1.44	1.17	1.63	1.79	1.50	1.34	1.43
Al ₂ O ₃	15.07	15.02	15.03	14.75	14.77	16.09	14.74	15.75	15.09
Fe ₂ O ₃	11.81	11.28	12.11	11.08	13.03	11.42	12.34	11.14	12.08
MnO	0.16	0.15	0.17	0.15	0.18	0.16	0.17	0.16	0.16
MgO	7.92	8.44	9.19	8.60	10.47	6.20	8.61	6.40	8.01
CaO	9.30	9.44	9.04	9.12	9.08	9.76	8.95	9.65	8.13
Na ₂ O	2.92	3.15	2.97	2.62	2.92	3.18	2.83	2.76	3.09
K ₂ O	0.53	0.48	0.73	0.50	0.84	0.75	0.76	0.62	0.69
P ₂ O ₅	0.17	0.15	0.22	0.16	0.28	0.27	0.21	0.18	0.20
Total	101.84	100.82	100.64	99.91	101.20	100.71	100.84	100.55	101.04
⁸⁷ Sr/ ⁸⁶ Sr	0.705517±9	0.705544±9	0.705566±9	0.705400±10	0.705456±8	0.704864±8	0.704725±7	0.705503±9	0.706003±10
¹⁴³ Nd/ ¹⁴⁴ Nd	0.512711±5	0.512719±4	0.512701±15	0.512618±7	0.512379	0.512913	0.512681	0.512625±6	0.512589±5
La	10.27	9.01	13.54	9.06	15.88	16.02	11.91	11.81	13.08
Ce	22.15	19.53	29.24	19.84	33.82	34.29	25.9	25.57	28.46
Nd	12.721	11.224	15.891	11.451	17.989	19.019	14.517	14.074	15.575
Sm	3.398	3.014	3.923	2.998	4.179	4.734	3.771	3.570	3.938
Eu	1.130	1.055	1.292	1.046	1.376	1.581	1.272	1.215	1.314
Gd	3.993	3.499	4.325	3.405	4.423	5.163	4.295	3.994	4.404
Dy	3.867	3.479	4.254	3.355	4.148	4.865	4.250	3.939	4.303
Er	2.116	1.910	2.347	1.838	2.256	2.599	2.327	2.177	2.385
Yb	1.861	1.671	2.094	1.639	1.999	2.246	2.047	1.950	2.144
Lu	0.266	0.239	0.301	0.235	0.289	0.319	0.293	0.281	0.309
²³⁰ Th/ ²³² Th		0.982±8	1.004±13	0.926±5				1.037±8	
²³⁰ Th/ ²³⁸ U		1.038±9	1.086±14	1.041±6				1.044±8	
²³⁸ U/ ²³² Th		0.945±05	0.924±2	0.889±07				0.993±1	
Th		1.555	2.149	1.344				1.718	
U		0.484	0.655	0.394				0.562	

Isotopic and REE (ppm) data produced for this study are in **Bold**, except values from Menzies et al. (1991).

5.2. Crustal contamination versus mantle heterogeneity

Isotopic and trace element data for the ZBVF lava flows support the involvement of at least two distinct isotopic sources prior to eruption. Whereas the range in radiogenic isotopic ratios is restricted and comparable to that observed in oceanic basalts (Fig. 6), [e.g. compiled OIB isotopic data from Reisberg et al. (1993) and McKenzie and O'Nions (1998)], the ZBVF lava flows are clearly not primitive and have erupted through Proterozoic (?) mantle and Proterozoic crust. Consequently assimilation, as well as fractional crystallisation processes (i.e. AFC), may have contributed to the observed elemental and isotopic heterogeneity.

5.2.1. Qualitative observations

The effects of AFC processes in the ZBVF lava flows can be evaluated through recognition of specific correlations between element abundances, element

ratios, and isotopic ratios. With progressive fractionation and decreasing MgO and increasing SiO₂ wt.%, an increase in characteristics associated with assimilation of a felsic and isotopically aging crustal end-member, e.g. Sr depletion, higher ⁸⁷Sr/⁸⁶Sr, and lower ¹⁴³Nd/¹⁴⁴Nd, should help identify any associated crustal assimilation.

⁸⁷Sr/⁸⁶Sr ratios for the ZBVF lava flows display a positive correlation with 1/Sr (Fig. 7a) (or a negative correlation with Sr), and Rb/Sr (Fig. 7b), possibly indicative of AFC-type processes. However, Menzies et al. (1991) noted that such trends among ⁸⁷Sr/⁸⁶Sr, Sr, and Rb/Sr exist in both the ZBVF lavas and in uncontaminated ocean island volcanic rocks from Oahu, Hawaii. Further more, a positive correlation of ⁸⁷Sr/⁸⁶Sr and Rb/Sr was ascribed by Perry et al. (1987) to variable degrees of melting from an isotopically enriched lithospheric and depleted asthenospheric mantle source. Fig. 4 displays a general increase in Sr concentration with

QBM803	QBB301	QBB901a	QBP601	QBP602	QVT301	QV805	QB802	QBO607
McCartys	Bandera	Bandera	Paxton Springs	Paxton Springs	Twin Crater	Cinder Field	Older Basalts	Oso Ridge
Tholeiite	Alkali	Alkali	Alkali	Alkali	Alkali	Alkali	Alkali	Alkali
51.56	45.38	46.25	46.03	45.93	45.60	46.34	46.86	45.47
1.36	2.27	2.23	2.19	2.21	2.56	2.43	2.28	2.81
15.36	14.60	14.79	14.50	14.48	14.60	14.58	14.55	15.50
11.46	12.66	12.18	12.63	12.76	12.69	12.51	11.92	14.29
0.16	0.18	0.17	0.18	0.18	0.17	0.18	0.17	0.16
8.05	10.30	10.43	11.15	10.84	9.56	10.24	10.23	5.89
9.37	9.40	9.39	9.72	9.73	8.98	8.92	8.85	7.47
2.89	3.30	3.28	2.85	2.80	3.52	3.43	3.39	5.34
0.70	1.40	1.39	1.35	1.32	1.64	1.59	1.68	2.39
0.19	0.52	0.51	0.45	0.46	0.58	0.60	0.58	0.96
101.10	100.01	100.62	101.05	100.71	99.90	100.82	100.51	100.28
0.705749±12	0.703625±10	0.703639±7	0.703788±8	0.703770±10	0.703288±6	0.703414±10	0.703407±9	0.702986±9
0.512694±7	0.51289±6	0.512712	0.512845±5	0.512841±33	0.512891±6	0.512901±4		0.512978
12.44	29.01	28.14	24.5	24.86	31.9	31.73	21.18	60.05
26.87	59.44	57.8	51.71	52.6	66.06	65.04	43.18	120.98
14.648	29.472	28.850	26.318	26.691	33.061	31.794	20.863	56.912
3.680	6.201	6.103	5.650	5.729	6.964	6.552	4.281	11.129
1.242	1.990	1.964	1.801	1.824	2.231	2.088	1.371	3.460
4.095	5.811	5.735	5.459	5.508	6.335	5.992	3.937	8.884
4.000	4.650	4.598	4.575	4.596	4.763	4.712	3.206	4.923
2.211	2.257	2.228	2.302	2.313	2.140	2.216	1.545	1.411
1.985	1.874	1.852	1.937	1.944	1.678	1.787	1.273	0.800
0.286	0.266	0.264	0.275	0.276	0.233	0.251	0.179	0.102
							1.219±8	1.281±10
							1.077±7	1.144±9
							1.131±1	1.120±1
							2.303	5.531
							0.859	0.204

decreasing MgO wt.% for both alkali and tholeiite basalts, a trend paralleled by other incompatible elements (Fig. 4). This supports interpretations of isotopic and chemical compositional variability as a result of partial melting and fractional crystallisation rather than assimilation of high $^{87}\text{Sr}/^{86}\text{Sr}$ crustal material.

On the plot of $^{143}\text{Nd}/^{144}\text{Nd}$ against SiO_2 (Fig. 7c), the ZBVF rocks form discrete clouds with no obvious correlation between Nd isotope ratios and usual elemental measures of magma differentiation. Viewed individually, the alkali basalts plot as a restricted group, suggesting that fractionation and assimilation processes were minimal to non-existent during ascent. The tholeiite basalts, however, show greater variability in both $^{143}\text{Nd}/^{144}\text{Nd}$ and SiO_2 , with no observable trend. The lack of correlation between the major element and isotopic data suggests that the isotopic compositions were inherited from variations in mantle source regions, and that they did not change during fractionation.

Fig. 7d shows a range in $^{87}\text{Sr}/^{86}\text{Sr}$ at constant MgO wt.% for the tholeiitic rocks. The alkali basalts plot on a roughly positive linear trend where a restricted and depleted-mantle-like range in $^{87}\text{Sr}/^{86}\text{Sr}$ is coupled to a 6–11 wt.% variation in MgO. One would expect a negative trend of decreasing MgO with increasing $^{87}\text{Sr}/^{86}\text{Sr}$ should AFC type processes have occurred. The lack any of such trend allows us to propose closed-system fractionation during ascent. Furthermore, for both suites, a general negative correlation between $^{143}\text{Nd}/^{144}\text{Nd}$ and MgO (Fig. 7e), where the highest $^{143}\text{Nd}/^{144}\text{Nd}$ ratio is coupled with the lowest MgO value, strongly contradicts the expected trends of AFC processes. AFC processes involving fractionation (MgO decline) and typical crust with low $^{143}\text{Nd}/^{144}\text{Nd}$ would produce a positive correlation in Fig. 7e. Also, the poor correlation between MgO and $^{87}\text{Sr}/^{86}\text{Sr}$ (Fig. 7d) suggests that assimilation was not an important process, unless $^{87}\text{Sr}/^{86}\text{Sr}$ mantle was similar to $^{87}\text{Sr}/^{86}\text{Sr}$ crust,

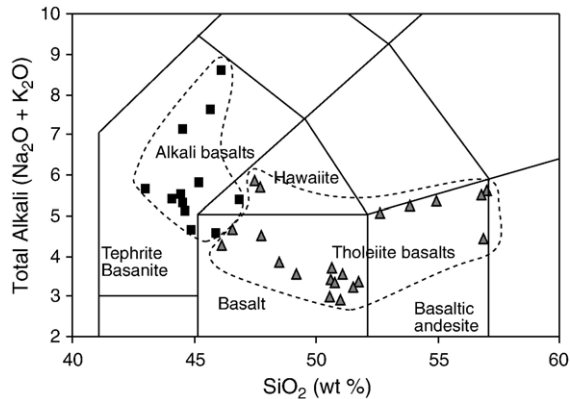


Fig. 2. Total alkalis vs. silica diagram (Le Bas et al., 1986) highlighting the range of silica saturation for the Zuni-Bandera lavas. Triangles = Tholeiites, Squares = Alkali basalts.

which could be possible if the lavas encountered granulite-facies crust. However, the $^{143}\text{Nd}/^{144}\text{Nd}$ ratios of the crust should remain un-altered during granulite-facies metamorphism and assimilation of such material would be observed in the ZBVF lava flows by significantly reduced $^{143}\text{Nd}/^{144}\text{Nd}$ values, a feature that is not observed.

Finally, the Colorado Plateau crust is characterised by a relatively high abundance of intermediate and mafic rocks, comparable to exposed arcs accreted onto continents, although more enriched in incompatible elements (Condie and Selverstone, 1999). As with all arc-derived material, subduction geochemical signatures are observed, particularly Nb and Ta depletions and a strong enrichment in Pb. Primitive-mantle-normalised diagrams show that the alkali basalts have relative depletions in Pb and enrichments in Nb, contradictory to the chemical characteristics of the crust (Fig. 5).

5.2.2. Quantitative modelling

Bulk-mixing trajectories, akin to magma mixing (Fig. 7f) have been produced to simulate contamination of the ZBVF lava flows through bulk assimilation of lower- and upper-crustal end-members that contain time-integrated enriched Sr–Nd isotopic ratios. Isotopic data for crustal xenoliths has been produced by Wendlandt et al. (1993), and Condie et al. (1999), with data for the ZBVF lava flows produced by Menzies et al. (1991), and this study. Crustal xenoliths MT-6, RM-3, SR-4, and TH-10A from Condie et al. (1999) and 86MR29, 86MR30, 88MR6, and 88R23 from Wendlandt et al. (1993) produced the best correlations with the ZBVF isotopic array. Crustal xenoliths for both studies were

collected from the Colorado Plateau in the Four Corners region of Colorado, Utah, Arizona, and New Mexico. Samples MT-6, RM-3, SR-4, and TH-10A from Condie et al. (1999) are Proterozoic granitoids representing the upper-crust, while samples 86MR29, 86MR30, 88MR6, and 88R23 from Wendlandt et al. (1993) are paragneiss meta-sedimentary rocks representing the lower-crust. Crustal xenoliths from Wendlandt et al. (1993) and Condie et al. (1999) highlight the heterogeneous isotopic composition of the crust: $^{87}\text{Sr}/^{86}\text{Sr}$ 0.71189 to 0.8165; $^{143}\text{Nd}/^{144}\text{Nd}$ 0.512138 to 0.510731. If we assume that all ZBVF lava flows originate from a single long-term depleted source, depending on the crustal material encountered, values of 30% to 50% contamination would be required to have produced the isotopically enriched ratios in the ZBVF tholeiites.

However, values of 30% to 50% assimilation would significantly elevate the concentrations of LIL and LRE elements, with associated crustal characteristics becoming strongly inherited in the major elements; these expectations are inconsistent with the mafic nature and observed elemental abundances in the volcanic rocks. It is therefore concluded that although the ZBVF magmas ascended through Proterozoic continental crust, the involvement of crustal rocks, evaluated through AFC processes was negligible during ascent. It is important to note that the heterogeneous chemistry of the Colorado Plateau makes modelling of bulk mixing and AFC processes difficult to evaluate. Chemical heterogeneity inherited from sub-Moho depths is consistent with the conclusions of Menzies and Kyle (1990) and Menzies et al. (1991) that the association of increasing $^{87}\text{Sr}/^{86}\text{Sr}$ with increasing Rb/Sr and other VICE/MICE ratios (very incompatible elements/moderate incompatible elements), for the ZBVF lava flows is best explained by variable degrees of partial melting from heterogeneous mantle sources.

5.3. Origin of lithospheric mantle heterogeneity

Lithospheric mantle heterogeneity beneath the Colorado Plateau has been investigated using petrological, geochemical (Kempton et al., 1987), and isotopic (Menzies et al., 1985) data from xenoliths entrained in alkali basalts from the Geronimo Volcanic Field, Arizona, USA. In general, a depleted spinel–peridotite protolith ($^{87}\text{Sr}/^{86}\text{Sr}=0.703$) was produced and stabilized in the Archaean (?) and Proterozoic and subsequently enriched ($^{87}\text{Sr}/^{86}\text{Sr}<0.706$) during the Proterozoic and Phanerozoic by upwelling of melts relating to supra-subduction processes, plume contamination (Yellowstone), and

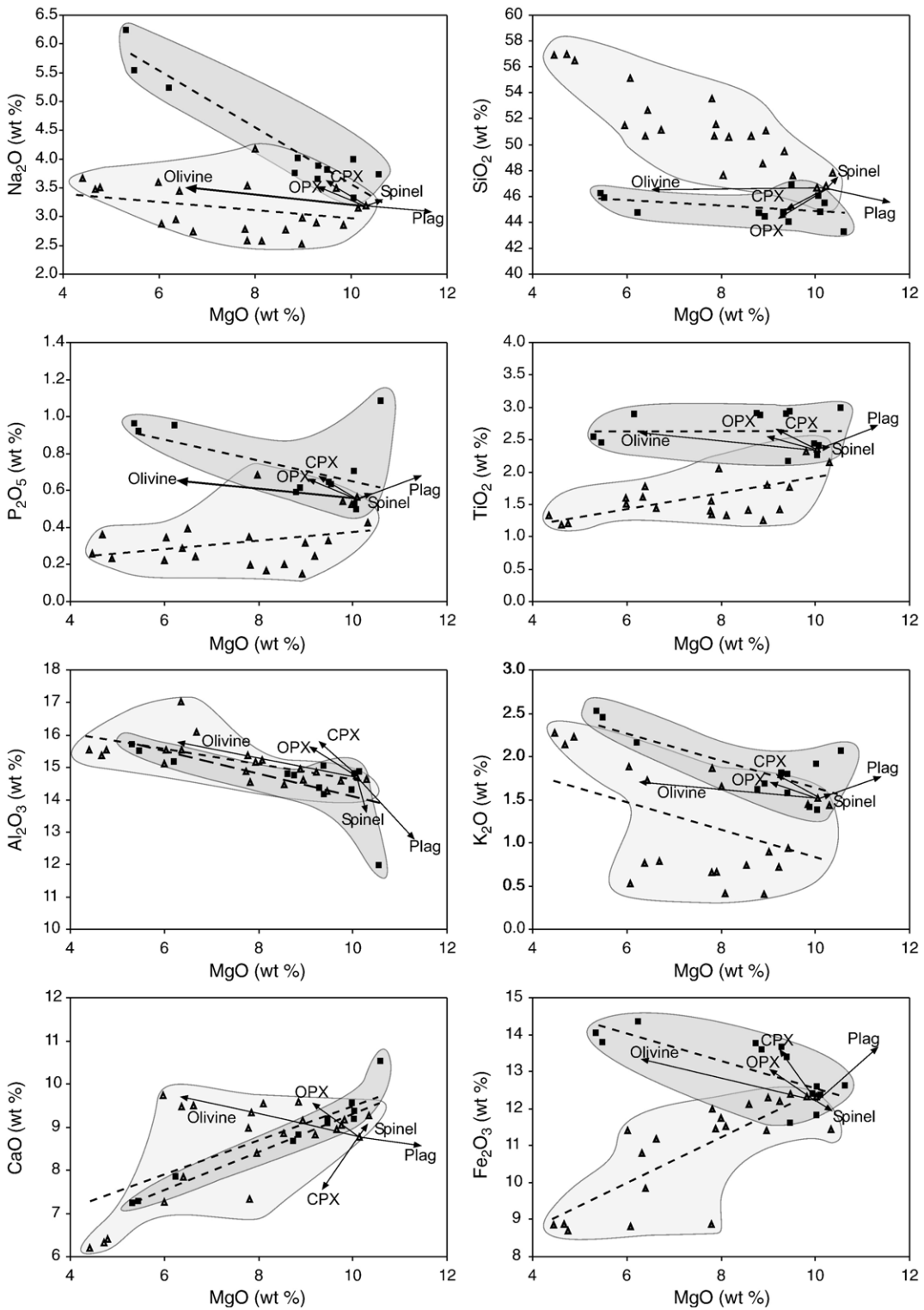


Fig. 3. MgO vs. major element data for the ZBFV. Diagrams are annotated with 10% fractional crystallization vectors to show the dominance of a clinopyroxene and olivine assemblage. The vectors begin at an assumed primitive sample and move away on a trend calculated to represent the change in sample composition with removal of 10% of each individual mineral. Triangles=tholeiite basalts, Squares = alkali basalts.

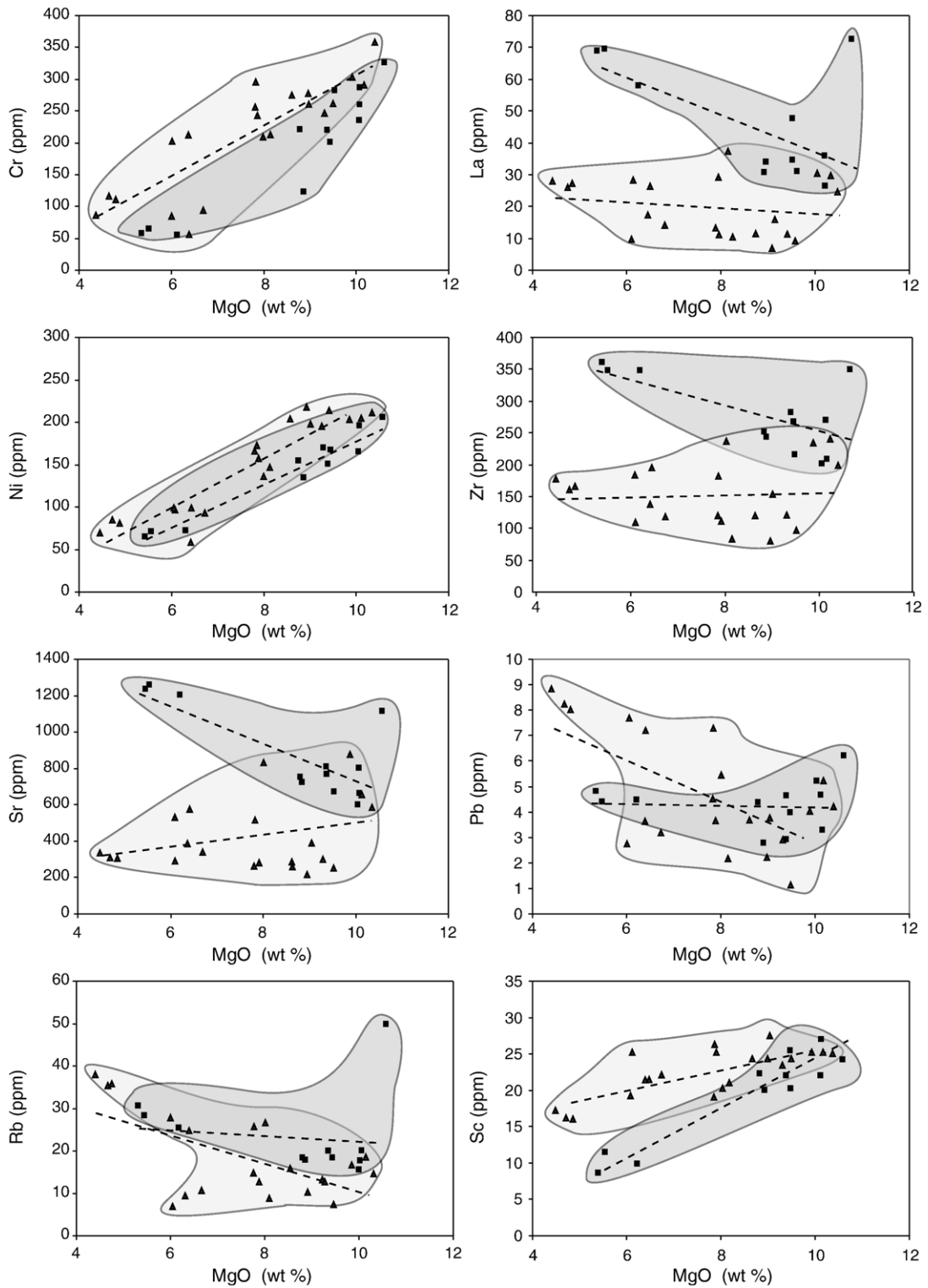


Fig. 4. MgO vs. trace element data for the ZBVF. Positive and negative correlations generally display the effect of fractional crystallization on the lavas. Triangles = tholeiite basalts, Squares = alkali basalts.

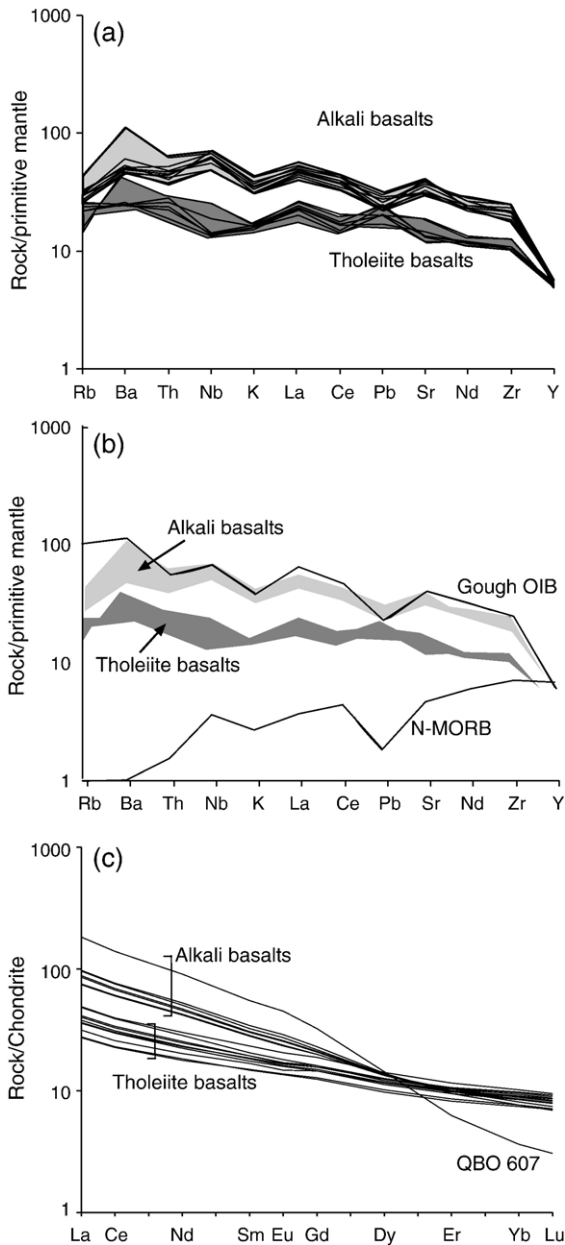


Fig. 5. (a) Primitive-mantle-normalized plots for representative alkali and tholeiite basalt samples from the ZBVF. (b) Comparison of ZBVF samples with ocean island basalt, represented by values from Gough, and mid ocean ridge basalts represented by N-MORB. Primitive mantle, Gough, and N-MORB values are from Sun and McDonough (1989). (c) Chondrite-normalized rare earth element profiles for the representatives of the ZBVF. Chondrite values are from Nakamura (1974).

infiltration of asthenospheric melts (Menzies, 1990; Menzies et al., 1991). The composition of the deeper lower lithosphere is represented by LREE and isotopically “enriched” ($^{87}\text{Sr}/^{86}\text{Sr} < 0.706$) garnet–peridotite xenoliths

from the Navajo Volcanic Field, central Colorado Plateau (Roden et al., 1990). The composition of the underlying asthenosphere appears to be similar to MORB, with an $^{87}\text{Sr}/^{86}\text{Sr}$ ratio range = 0.702 to 0.703 as exemplified by alkali basalts from throughout the Basin and Range province (Menzies et al., 1983; Perry et al., 1988; Kempton et al., 1991).

6. Mantle processes

If we accept that the chemical heterogeneity in some of the ZBVF lavas has been unaffected by AFC processes, then we can begin to explore the origin of the ZBVF magmas through partial melting of sub-Moho sources in the lower lithosphere and asthenosphere.

6.1. Modelling partial melting and REE ratios

Semi-quantitative partial melting models (Fig. 8abc) using REE ratios have been calculated to constrain the extent and depth of partial melting, along with the facies mineralogy and chemistry, using the methodologies of Thirlwall et al. (1994) and Shaw et al. (2003), and partition coefficients from McKenzie and O’Nions (1991). With partial melting from either spinel- or garnet-facies peridotite, the LREE (e.g. La) will be enriched in the melt to produce La/Yb variations with variable degrees of partial melting. Garnet-facies melts will produce higher La/Yb ratios relative to spinel-facies melts. Enrichment in MREE (e.g. Dy) relative to HREE (e.g. Yb) occurs only where garnet is a residual phase during partial melting, and the HREE (Yb) are preferentially retained by garnet (high $D_{\text{Yb}} \sim 40\text{--}15$) relative to the MREE (Dy). Thus, increasing MREE/HREE (Dy/Yb) ratios develop with decreasing degrees of partial melting within the garnet-facies, producing large differences between source and melt ratios. In contrast, melting of a spinel peridotite will result in a minimal variation in MREE/HREE (Dy/Yb) ratios with melt fraction because $D_{\text{Dy}}^{\text{Cpx}}$ is near-equal to $D_{\text{Yb}}^{\text{Cpx}}$ (McKenzie and O’Nions, 1991), even in near sub-solidus clinopyroxene (Blundy et al., 1998), and the melt and source ratios will be comparable. The relative contribution of each facies can be identified using a plot of $(\text{Dy}/\text{Yb})_{\text{N}}$ vs. $(\text{La}/\text{Yb})_{\text{N}}$. On such plots (Fig. 8ab) the denominator for each ratio remains the same (Yb) and mixing between melts from each facies will produce linear arrays (Hanson and Langmuir, 1978) with varying phase contributions and degrees of partial melting (Thirlwall et al., 1994). Fig. 8a displays a plot of $(\text{Dy}/\text{Yb})_{\text{N}}$ against $(\text{La}/\text{Yb})_{\text{N}}$ for the ZBVF, along with modelled trajectories for non-modal fractional melts of

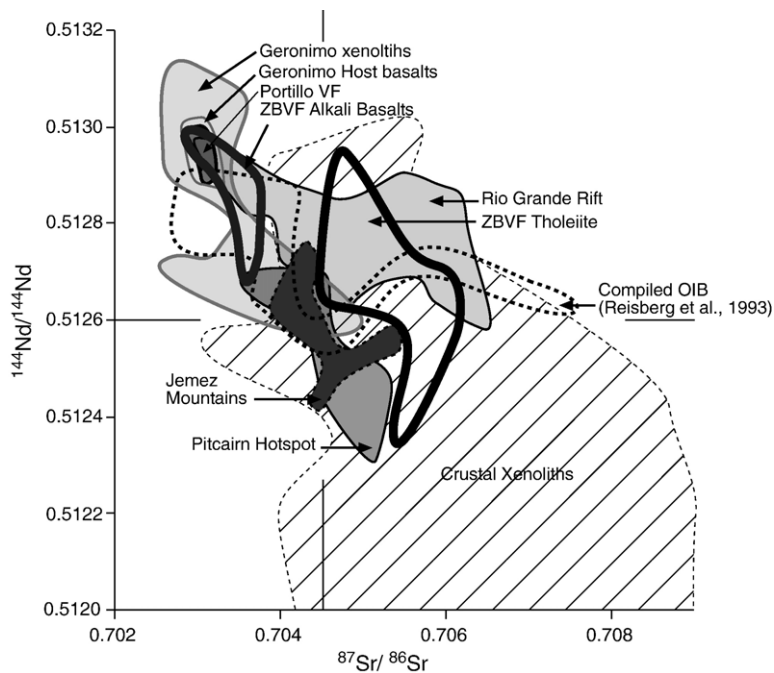


Fig. 6. $^{87}\text{Sr}/^{86}\text{Sr}$ vs. $^{144}\text{Nd}/^{144}\text{Nd}$ for the ZBVF data from this study and Menzies et al. (1991). Crustal xenolith data from Wendlandt et al. (1993) and Condie et al. (1999). Geronimo Volcanic Field data from Menzies et al. (1985). Potrillo Volcanic Field data from Thompson et al. (2005). Pre-caldera mafic lavas of the Jemez Mountains on the Jemez Lineament data from Wolff et al. (2005), Rio Grande Rift data from Perry et al. (1987), OIB data compiled from Reisberg et al. (1993) and McKenzie and O’Nions (1998) (references therein).

garnet- and spinel-peridotite sources. The source is a primitive mantle composition (Sun and McDonough, 1989) as a crude approximation to begin modelling.

Variations in the degree of partial melting involving a spinel or garnet peridotite alone cannot produce the observed variation between $(\text{Dy}/\text{Yb})_N$ and $(\text{La}/\text{Yb})_N$ (Fig. 8a) for the ZBVF. Spinel peridotite melts alone are not capable of producing the large co-variation between $(\text{Dy}/\text{Yb})_N$ and $(\text{La}/\text{Yb})_N$, while variable degrees of melting involving a garnet peridotite alone would require an unrealistic high degree of melting to produce the minimum $(\text{Dy}/\text{Yb})_N$. The alkali basalts clearly display a range in $(\text{Dy}/\text{Yb})_N$ far outside that of a melt produced entirely within the spinel-facies, while the tholeiite basalts show a restricted range in $(\text{Dy}/\text{Yb})_N$ and $(\text{La}/\text{Yb})_N$ suggestive of an almost complete spinel-facies melt (Fig. 8a). However, variation in both suites follows the same positive correlation, suggesting that variable degrees of mixing between spinel- and garnet-facies melts occurred during petrogenesis of both basalt types.

Although the Yb (HREE and Y) concentrations in the ZBVF samples may in part be controlled by fractional crystallization of olivine and clinopyroxene, samples with comparable MgO wt.% have variable Yb concentrations (e.g. QV805 10.24 wt.% MgO and 1.787 ppm

Yb, QB802 10.23 wt.% MgO and 1.273 ppm Yb), with no observable correlation between Yb and MgO in the ZBVF samples. A negative hyperbolic correlation between La/Yb and Yb ppm (Fig. 8c) in the alkali basalts is inconsistent with variable degrees of melting from either a spinel- or a garnet-peridotite mantle alone, again suggesting mixing between spinel- and garnet-facies melts occurred during petrogenesis. Melting of garnet peridotite alone would produce melts that exhibit no co-variation between La/Yb and Yb ppm, as Yb is retained in the source. The tholeiite basalts plot away from the main trend line on a high angle trend exhibiting an array that parallels the spinel melting line. This supports melting for the tholeiite basalts involving a spinel-facies peridotite with little to no input from a garnet-facies peridotite.

The REE model (Fig. 8a) produced can accommodate almost all ZBVF samples except the most LREE enriched sample, QBO 607, which resides above the garnet-facies melting trajectory, intersecting on a trend at $\sim 0.75\%$ garnet-facies melting, with $(\text{Dy}/\text{Yb})_N$ and $(\text{La}/\text{Yb})_N$ ratios indicating melting of a garnet-facies peridotite alone.

Using a modelled bulk distribution coefficient ratio $D_{\text{Dy}}/D_{\text{Yb}}=0.24$, rather than $D_{\text{Dy}}/D_{\text{Yb}}=0.30$ from

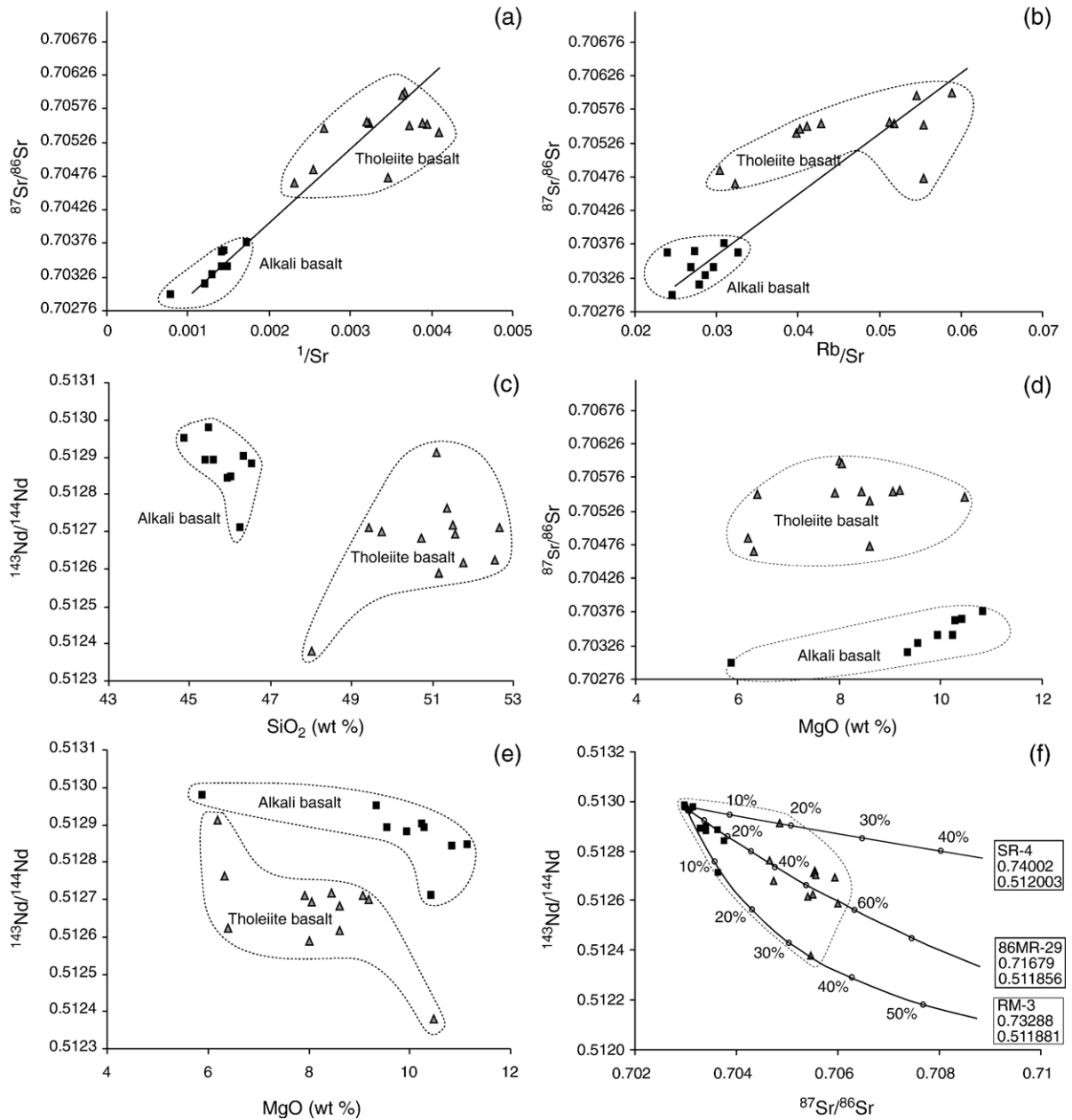


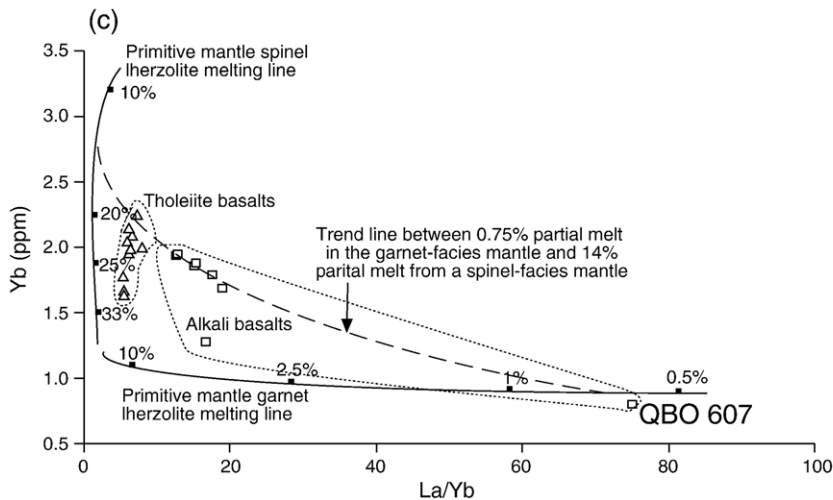
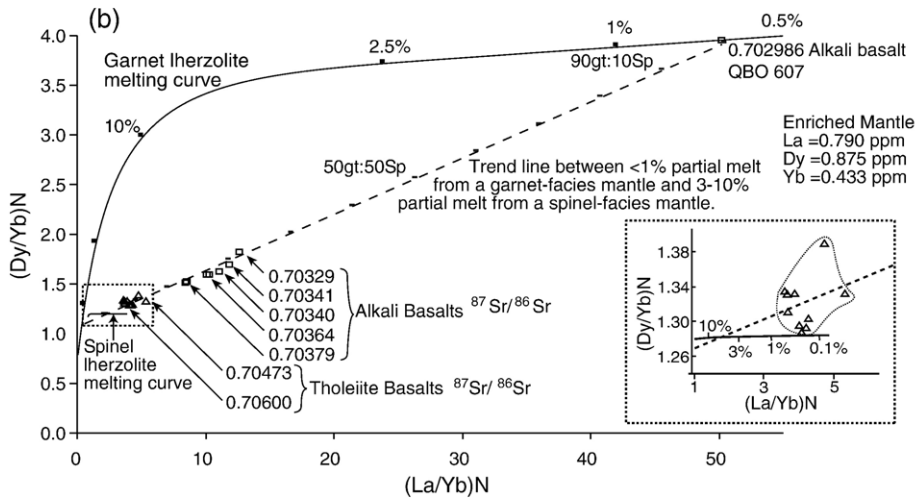
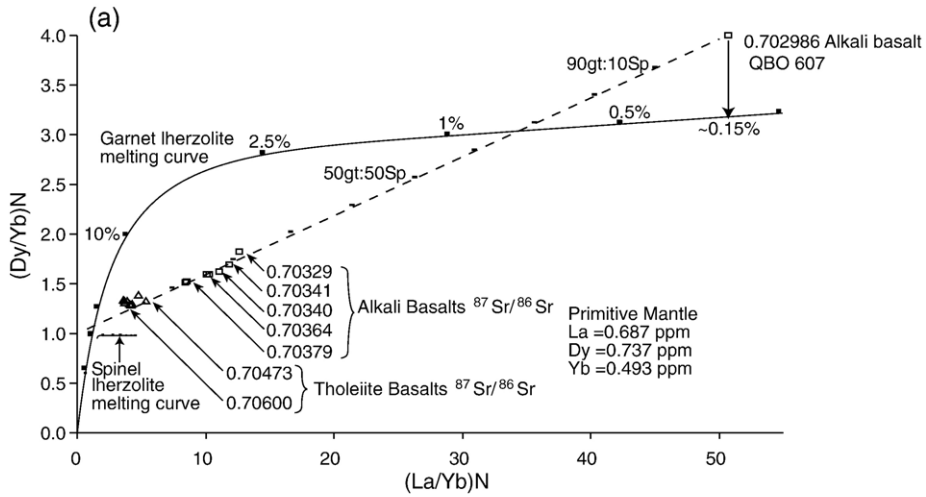
Fig. 7. (a) $^{87}\text{Sr}/^{86}\text{Sr}$ vs. $1/\text{Sr}$ concentration. (b) $^{87}\text{Sr}/^{86}\text{Sr}$ vs. Rb/Sr . (c) $^{143}\text{Nd}/^{144}\text{Nd}$ vs. SiO_2 wt.%. (d) $^{87}\text{Sr}/^{86}\text{Sr}$ vs. MgO wt.%. (e) $^{143}\text{Nd}/^{144}\text{Nd}$ vs. MgO wt.%. (f) $^{143}\text{Nd}/^{144}\text{Nd}$ vs. $^{87}\text{Sr}/^{86}\text{Sr}$. Bulk mixing is between a depleted sample from the ZBVF (QBO 607) and enriched crustal xenoliths (Wendlandt et al., 1993; Condie et al., 1999). Triangles = tholeiite basalts, Squares = alkali basalts.

McKenzie and O’Nions (1991), the garnet melting trajectory can easily accommodate sample QBO 607 as a primitive mantle melt. However, as noted by Shaw et al. (2003) published garnet distribution coefficients differ and the position of the trajectory is sensitive to such differences. Using compiled distribution coefficients from McKenzie and O’Nions (1991), the $(\text{Dy}/\text{Yb})\text{N}$ ratio of sample QBO 607 cannot be reproduced by varying

either the source mineralogy or the melting proportions, allowing the most probable explanation to reside within assumptions made about the composition of the mantle source (or measured distribution coefficients used during modelling). To evaluate the mantle source composition, raising the $(\text{Dy}/\text{Yb})\text{N}$ ratio of the primitive mantle source from ~ 0.95 to > 1.25 allows sample QBO 607 to plot as a 100% garnet-facies melt (Fig. 8b). This ratio can be

produced in the model by increasing the primitive mantle source Dy concentration by ~15% and decreasing the Yb concentration by ~12%, giving a 0.7% garnet-facies

melt for sample QBO 607. Such shifts in source composition could reflect metasomatic activity at the base of the lithosphere.



The $(\text{La}/\text{Yb})_N$ ratio of sample QBO 607 can be reproduced using a primitive mantle source ratio of $(\text{La}/\text{Yb})_N \sim 0.93$, to give a calculated 0.15% garnet-facies melt (Fig. 8a). The depleted isotopic ratios of sample QBO 607 suggest melting from a long-term LREE-depleted DMM source, but, modelling garnet-facies melting with an average DMM composition from Workman and Hart (2005) $(\text{La}/\text{Yb})_N = 0.35$ cannot reproduce sample QBO 607 even at $\ll 0.001\%$ melting. All alkali basalt samples display depleted $^{143}\text{Nd}/^{144}\text{Nd}$ and $^{87}\text{Sr}/^{86}\text{Sr}$ ratios relative to Bulk Earth ($^{143}\text{Nd}/^{144}\text{Nd} = 0.51264$ and $^{87}\text{Sr}/^{86}\text{Sr} \sim 0.7045$) supporting melting from a LREE-depleted source, although not as depleted as MORB source. Tholeiite basalts straddle the Bulk Earth $^{143}\text{Nd}/^{144}\text{Nd}$ ratio and plot above the Bulk Earth $^{87}\text{Sr}/^{86}\text{Sr}$, suggesting both LREE-enriched and -depleted sources were involved during melting. Involvement of a LREE and isotopically enriched mantle source could have arisen through melting at the base of the lithosphere, which has been isolated from mantle convection as to produce aged isotopic values [$^{87}\text{Sr}/^{86}\text{Sr} < 0.706$ (Menzies et al., 1991)], and has undergone metasomatic alteration, specifically from garnet-facies silicate fluids. To model the production of isotopically enriched tholeiite basalts as partial melts from a LREE-enriched source, starting with a primitive mantle composition (Sun and McDonough, 1989), $\sim 15\%$ source enrichment of La with an increased $(\text{Dy}/\text{Yb})_N$ of ~ 1.25 have been introduced into the model. The results indicate that the ZBVf samples define a trend that intersects the spinel-facies melting trajectory between 3–10% and the garnet-facies melting trajectory at $< 1\%$ melt ($\sim 0.7\%$ sample QBO 607) (Fig. 8b). With expansion of the tholeiite basalt suite and spinel-facies melting trajectory (Fig. 8b), vertical extrapolation of the sample points to the melting trajectory shows the tholeiite basalts to lie at $< 1\%$ melting. This compares with the $< 1\%$ melting value for the garnet-facies melting trajectory, produced by sample QBO 607. This is an expected result and implies that mantle melting beneath the ZBVf occurred without a mantle thermal anomaly. Consequently the amount of shallow mantle involved in polybaric

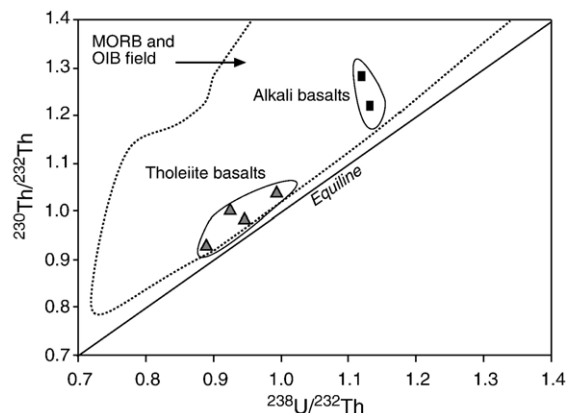


Fig. 9. U–Th isotopic data from the ZBVf, MORB and OIB field taken from Condomines and Sigmarsson (2000) (and references therein). Triangles represent tholeiite basalts and squares represent alkali basalts. Alkali basalts plot away from the equiline indicating a greater contribution of melt from a garnet-facies mantle.

melting remains the same allowing both suites to be produced at similar degrees of melting.

6.2. U–Th disequilibria

Further evidence of the relative contributions from spinel- and garnet-facies mantle sources can be identified from a plot of $(^{230}\text{Th}/^{232}\text{Th})$ vs. $(^{238}\text{U}/^{232}\text{Th})$ (Fig. 9). The ZBVf samples plot above the equiline indicating melting where (^{230}Th) is in excess of (^{238}U) . Experimental data by Beattie (1993) have showed that the ^{230}Th excess in MORB and most OIB, [observed in $(^{230}\text{Th}/^{238}\text{U})$ ratios] is best explained by near-fractional melting initiated in the garnet stability field at a slow melting rate. The ZBVf basalts display variable ^{230}Th excess. The alkali basalts have a $^{230}\text{Th}/^{238}\text{U}$ range of 1.07 to 1.14, and plot higher above the equiline than the tholeiite basalts which have a $^{230}\text{Th}/^{238}\text{U}$ range of 1.03 to 1.08. This indicates that the alkali basalts have an increased contribution of melt generated in the presence of garnet. Asmerom (1999) and Asmerom et al. (2000) reported U–Th–Pa isotopic data from volcanic rocks

Fig. 8. Calculated partial melting curves assuming non-modal fractional melting of garnet- and spinel-lherzolite sources. Garnet lherzolite: 0.598 ol, 0.211 opx, 0.076 cpx, 0.115 grt, that melts in the proportions 0.05 ol, 0.2 opx, 0.3 cpx, 0.45 grt; spinel lherzolite: 0.578 ol, 0.27 opx, 0.119 cpx, 0.033 sp, that melts in the proportions 0.1 ol, 0.27 opx, 0.5 cpx, 0.13 sp (Thirlwall et al., 1994). (a) to (b) $(\text{Dy}/\text{Yb})_N$ vs. $(\text{La}/\text{Yb})_N$ for the ZBVf. Analyses are normalized to chondrite using values from Nakamura (1974). (a) Melt curves use a primitive mantle composition from Sun and McDonough (1989). With a primitive-mantle source composition the trend of the ZBVf does not intersect the spinel lherzolite melting curve, nor can the garnet lherzolite melting curve accommodate sample QBO 607. (b) Melt curves have an enriched mantle composition with 15% enrichment in La and Dy, and 12% depletion in Yb. The dashed box surrounding the tholeiite basalts and the spinel lherzolite melting curve corresponds to the inserted graph with the dashed box outline. The inserted graph represents an enlargement of the spinel lherzolite melting curve to show the tholeiite basalts to lie on a trend of 3–10% spinel-facies melt and have $(\text{La}/\text{Yb})_N$ ratios to give an overall $< 1\%$ spinel-facies source melting. (c) La/Yb vs. Yb ppm for the ZBVf. Melt curves have a primitive mantle composition. Partition coefficients from McKenzie and O’Nions (1991). Figures (a) and (b) are annotated with Sr isotope ratio values. Triangles = Tholeiites, Squares = Alkali basalts.

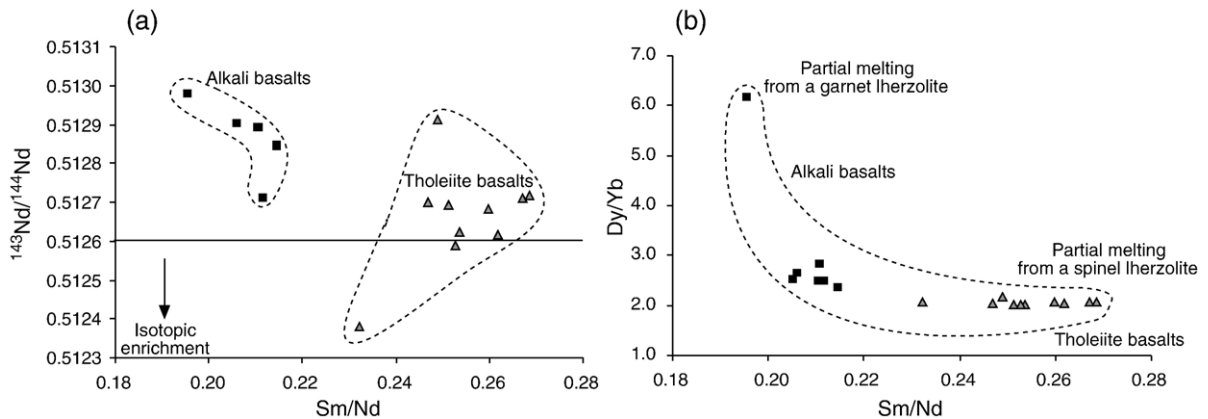


Fig. 10. (a) $^{143}\text{Nd}/^{144}\text{Nd}$ vs. Sm/Nd . The lowest Sm/Nd values correlate with depleted isotopic ratios for the ZBVF alkali basalts. (b) Dy/Yb vs. Sm/Nd . The lowest Sm/Nd values correlate with an increase in Dy/Yb . Hyperbola relationships highlight: (1) small degree partial melts from an isotopically depleted mantle (asthenosphere) source with an increased relative contribution from a garnet-facies mantle; and (2) partial melting from an isotopically enriched mantle reservoir (lithosphere?) with a significant contribution from a spinel-facies lherzolite. Triangles = Tholeiites, Squares = Alkali basalts.

across the western USA, and interpreted the ZBVF tholeiites as spinel-facies lithospheric melts, and the alkali basalts as garnet-facies asthenospheric melts. A general comparison with MORB and OIB data from [Condomines and Sigmarsson \(2000\)](#) (and references therein) places the ZBVF U–Th data within the oceanic array (Fig. 9), consistent with Sr and Nd isotopic data.

7. Potential end member compositions — the role of asthenospheric and lithospheric mantle sources

Models by [Menzies and Kyle \(1990\)](#) and [Menzies et al. \(1991\)](#) invoked sources located within the convecting asthenospheric mantle, with a depleted $^{87}\text{Sr}/^{86}\text{Sr}$ ratio < 0.703 , and an enriched source relating to either a lithospheric mantle or plume-contaminated asthenosphere mantle, with an $^{87}\text{Sr}/^{86}\text{Sr}$ ratio ~ 0.706 . Although the range in isotopic values observed in the ZBVF lava flows is comparable with the degree of compositional variability observed in oceanic basalts, this does not mean all ZBVF lava flows are restricted to an asthenospheric origin ([Fitton et al., 1991](#)). Consideration of REE modelling, the depth of the transition between spinel- and garnet-mantle facies, and the boundary between the lithosphere and asthenosphere, provides an insight into the location of specific mantle sources involved during genesis of the ZBVF.

Two components are apparent:

- a) A depleted mantle component that produced small-volume Ne-normative melts with $^{87}\text{Sr}/^{86}\text{Sr} = 0.7030$, $^{143}\text{Nd}/^{144}\text{Nd} = 0.51295$. It likely originated from a $< 1\%$ garnet-facies peridotite melt, with a reduced

contribution of a $< 1\%$ melt from spinel-facies peridotite. Trace element characteristics include $\text{Sr} > 1200$ ppm, $(\text{La}/\text{Yb})_N = 12.7$ to 75.1, $(\text{Dy}/\text{Yb})_N = 2.4$ to 6.2, and $\text{Sm}/\text{Nd} = 0.21$.

- b) An enriched mantle component that produced large volume Hy-normative melts with $^{87}\text{Sr}/^{86}\text{Sr} = 0.70465$ to 0.70600, $^{143}\text{Nd}/^{144}\text{Nd} = 0.51240$ to 0.51291. It likely originated from a $< 1\%$ melt from spinel-facies peridotite, with little to no contribution from a $< 1\%$ garnet-facies peridotite melt. Trace element characteristics include $\text{Sr} = 400$ ppm, $(\text{La}/\text{Yb})_N = 5.4$ to 7.9, $(\text{Dy}/\text{Yb})_N = 2.0$ to 2.16, and $\text{Sm}/\text{Nd} > 0.26$.

7.1. The role of the lithospheric mantle

The lithospheric mantle consists of two parts, as discussed by [McKenzie and Bickle \(1988\)](#). The upper part is mechanically rigid, transports thermal energy by conduction, and referred to as the Mechanical Boundary Layer (MBL). The MBL is separated from the convectively mixing asthenosphere, and thus can act as a repository for isotopic systems to accumulate radiogenic daughter nuclides, leading to isotopically enriched mantle sources with time. Below the MBL there exists a Thermal Boundary Layer (TBL), a transition zone between the mechanically stable lithosphere and convecting asthenosphere, believed to have the composition of isotopically depleted MORB ([McKenzie and Bickle, 1988](#)).

Recent teleseismic data from [West et al. \(2004\)](#) reveals the velocity structure of the lithosphere from the Colorado Plateau across the Rio Grande Rift; part of the Rio Grande Rift Seismic Transect Experiment (LA

RISTRA) seismic array in the southwest USA. The interpretation of the velocity structure reveals a transition in lithospheric thickness from 120–150 km beneath the Colorado Plateau to 45–55 km beneath the Rio Grande Rift. With the spinel-to garnet-transition at a depth of ~80 km (20–26 kbar) (Takahashi and Kushiro, 1983), one can infer that spinel–peridotite facies (<80 km) comprises most of the lower lithosphere beneath the Rio Grande Rift [where the lithosphere is very thin] and the ZBVF [where it is thicker]. Garnet-peridotite facies mantle (>80 km) is primarily part of the asthenosphere beneath the ZBVF. Modelling of the tholeiite basalt source shows a dominant contribution from spinel-facies mantle (95–100%), with olivine and clinopyroxene fractionation at low pressures and geochemical and isotopic similarities to OIB tholeiites. One can infer that tholeiitic melt production occurred within the lithospheric mantle.

7.2. The role of the asthenospheric mantle

Alkali basalt Sr–Nd isotopic ratios similar to MORB are compatible with the asthenosphere as a melt source. Long-term depleted (asthenospheric DMM) mantle sources develop high $^{143}\text{Nd}/^{144}\text{Nd}$ due to time-integrated high Sm/Nd ratios. A general, although weak ($R^2=0.4524$), correlation between $^{143}\text{Nd}/^{144}\text{Nd}$ and Sm/Nd is observed in the isotopically depleted ZBVF alkali basalt samples, which have the lowest Sm/Nd values (Fig. 10a). Chen and Frey (1983) and Shaw et al. (2003) interpret similar trends in terms of alkali basalts as forming by small degrees of melting (<1%) of a depleted source. While the trend observed in Fig. 10a is weak, correlations between MREE/HREE ratios (e.g. Dy/Yb) and Sm/Nd ratios (Fig. 10b) further substantiate the assertion that the alkali basalts are small degree partial melts from an isotopically depleted asthenospheric source in the presence of garnet.

The most favourable model to explain the ZBVF chemistry involves development of polybaric melting columns that straddle the lithosphere–asthenosphere boundary at 80–100 km, and contain a mix of melts from both spinel (<80 km) and garnet (>80 km) facies mantle. The depth range of the melt column and its position relative to the spinel-to garnet-facies boundary effectively controls the compositional variability in REE chemistry, particularly HREE. An influx of garnet-facies small-volume alkaline melts derived from the low-velocity structure could conceivably have mixed with spinel-facies, larger-volume, tholeiitic melts derived from the lithosphere. Consideration of U–Th data, Sr–Nd isotopic data, depth of mantle phase boundaries, and

lithospheric boundary parameters, allows us to propose that the portion of the melting column for the tholeiite basalts resided within the lower lithosphere, whereas the portion for the alkali basalts was at the base of the lithosphere and within the asthenosphere. While the alkaline melts may well have been derived from the low-velocity structure beneath the Rio Grande rift (West et al., 2004), it is not known to what extent the lower lithosphere beneath the Colorado Plateau was involved in the melting process. One could conceive of a situation where the only source of high $^{87}\text{Sr}/^{86}\text{Sr}$ and low $^{143}\text{Nd}/^{144}\text{Nd}$ isotope ratios beneath the ZBVF and the Jemez Lineament resides beneath the edge of the Colorado Plateau, known to have a high velocity structure that extends westward beneath the Colorado plateau to form a lithospheric mantle lid (West et al., 2004), and as such a greater chance of having preserved aged isotopes.

Such a model accounts for the following geochemical features: (1) the near-linear array observed though a plot of $(\text{Dy}/\text{Yb})_N$ against $(\text{La}/\text{Yb})_N$; (2) $(\text{Dy}/\text{Yb})_N$ ratios intermediate between those produced by melting of a garnet- and spinel-facies mantle alone; (3) the negative correlation between La/Yb and Yb concentration in the alkali basalts, and the vertical correlation in the tholeiite basalts; (4) the shift towards ^{230}Th excess observed in the alkali basalts; and (5) the enriched and depleted Sr–Nd isotope ratios concluded to be inherited from sub-Moho depths.

8. Summary and conclusions

Alkali and tholeiitic magmas of the ZBVF ascended through the Proterozoic continental crust of the Colorado Plateau, with the latter having undergone shallow-level fractional crystallization of olivine ± clinopyroxene ± spinel. The alkaline–tholeiitic lava flows lack elemental and isotopic correlations usually indicative of AFC and appear to have inherited their geochemistry from sub-Moho depths.

Nd–Sr isotopic data, partial melt modelling of REE, and U–Th disequilibria allows us to unravel the ZBVF mantle melting history. The compositions of the ZBVF lava flows are consistent with a model of polybaric melting, with mixing of melts over an extended depth range in melting columns that span both (a) the garnet- and spinel-facies phase boundaries in the mantle, and (b) the asthenosphere–lithosphere boundary, and (c) may have tapped Rio Grande asthenosphere and the lower lithosphere beneath the Colorado Plateau. Relative to a primitive mantle composition, the ZBVF lava flows can be modelled to originate from a source that underwent ~15% LREE and ~15% MREE enrichment with

~12% HREE depletion, likely relating to melting in the lower lithosphere. The tholeiite basalts are primarily spinel-facies mantle melts (95–100%) from <1% source melting, whereas the alkali basalts have a higher proportion of a <1% garnet-facies mantle melt (15–25% contribution for all samples except QBO 607 assumed to be 100% garnet-facies melt).

Acknowledgements

Thoughtful editorial reviews and handling from Jim Luhr, Nancy McMillan, Yi-Gang Xu, and Lang Farmer greatly improved the quality of the final manuscript. Constructive comments by Andy Saunders (Leicester) and Dave Matthey (Royal Holloway) helped improve the MSc thesis that formed the basis for this paper. Christina Manning (Royal Holloway) is thanked for her help and assistance with production of XRF data and Emily Proctor and John Fisher (Royal Holloway) are thanked for advice with production of graphics and figures.

References

- Anders, M., Heiken, G., Eichelberger, J., Laughlin, A., Huestis, S., 1981. Geologic and geophysical investigations of the Zuni–Bandera volcanic field, New Mexico. Los Alamos National Laboratory Report LA 8827-MS.
- Asmerom, Y., 1999. Th–U fractionation and mantle structure. *Earth and Planetary Science Letters* 166, 163–175.
- Asmerom, Y., Cheng, H., Thomas, R., Hirschmann, M., Edwards, R.L., 2000. Melting of the Earth's lithospheric mantle inferred from protactinium±thorium±uranium isotopic data. *Nature* 406, 293–296.
- Baldrige, W.S., Perry, F.V., Vaniman, D.T., Nealey, L.D., Leavy, B.D., Laughlin, A.W., Kyle, P., Bartov, Y., Steinitz, G., Gladney, E.S., 1991. Middle to late Cenozoic magmatism of the southeastern Colorado Plateau and Central Rio Grande rift (New Mexico and Arizona, U.S.A.): a model for continental rifting. In: Gangi, A.F. (Ed.), *World Rift Systems. Tectonophysics*, vol. 197, pp. 327–354.
- Beattie, B.D., 1993. Uranium–thorium disequilibria and partitioning on melting garnet peridotite. *Nature* 363, 63–65.
- Blundy, J.D., Robinson, J.A.C., Wood, B.J., 1998. Heavy REE are compatible in clinopyroxene on the spinel lherzolite solidus. *Earth and Planetary Science Letters* 160, 493–504.
- Chen, C.Y., Frey, F.A., 1983. Origin of Hawaiian tholeiite and alkalic basalt. *Nature* 302, 785–789.
- Condie, K.C., Selverstone, J., 1999. The crust of the Colorado Plateau: new views of an old arc. *Journal of Geology* 107, 387–397.
- Condie, K.C., Latysh, N., Van Schmus, W.R., Kozuch, M., Selverstone, J., 1999. Geochemistry, Nd and Sr isotopes, and U/Pb zircon ages of granitoid and metasedimentary xenoliths from the Navajo Volcanic Field, Four Corners area, southwestern United States. *Chemical Geology* 156, 95–133.
- Condomines, M., Sigmarsson, O., 2000. ²³⁸U–²³⁰Th disequilibria and mantle melting processes: a discussion. *Chemical Geology* 162, 95–104.
- Eisele, J., Sharma, M., Galer, S.J.G., Blichert-Toft, J., Devey, C.W., Hofmann, A.W., 2002. The role of sediment recycling in EM-1 inferred from Os, Pb, Hf, Nd, Sr isotope and trace element systematics of the Pitcairn hotspot. *Earth and Planetary Science Letters* 196, 197–212.
- Fitton, J.G., James, D., Leeman, W.P., 1991. Basic magmatism associated with late Cenozoic extension in the Western United States: compositional variations in space and time. *Journal of Geophysical Research* 96, 13 693–13 712.
- Goff, F., Grigsby, C.O., 1982. Valles Caldera geothermal systems, New Mexico, U.S.A. *Journal of Hydrology* 56, 119–136.
- Hanson, G.N., Langmuir, C.H., 1978. Modelling of major elements in mantle–melt systems using trace element approaches. *Geochimica et Cosmochimica Acta* 42, 725–741.
- Kempton, P.D., Dungan, M.A., Blanchard, D.P., 1987. Petrology and geochemistry of xenolith-bearing alkalic basalts from the Geronimo Volcanic Field, southeast Arizona. Evidence for polybaric fractionation and implications for mantle heterogeneity. *Special Papers of the Geological Society of America* 215, 347–370.
- Kempton, P.D., Fitton, J.G., Hawkesworth, C.J., Ormerod, D.S., 1991. Isotopic and trace element constraints on the composition and evolution of the lithosphere beneath the Southwestern United States. *Journal of Geophysical Research* 96, 13717–13735.
- Klein, E.M., Langmuir, C.H., 1987. Global correlations of ocean ridge basalt chemistry with axial depth and crustal thickness. *Journal of Geophysical Research* 92, 8089–8115.
- Le Bas, M., Le Maitre, R., Streckeisen, A., Zanettin, B., 1986. A chemical classification of volcanic rocks based on the total alkali–silica diagram. *Journal of Petrology* 27, 745–750.
- Leeman, W.P., 1982. Tectonic and magmatic significance of strontium isotopic variations in Cenozoic volcanic rocks from the western United States. *Geological Society of America Bulletin* 93, 487–503.
- Lum, C.C.L., Leeman, W.P., Foland, K.A., Kargel, J.A., Fitton, J.G., 1989. Isotopic variations in continental basaltic lavas as indicators of mantle heterogeneity: examples from the western U.S. Cordillera. *Journal of Geophysical Research* 94, 7871–7884.
- Maxwell, C.H., 1986. Geological map of El Malpais lava field and surrounding areas, Cibola County, New Mexico: US Geological Survey Map I-1595, scale 1:62,500.
- McKenzie, D., Bickle, M.J., 1988. The volume and composition of melt generated by extension of the lithosphere. *Journal of Petrology* 29, 625–679.
- McKenzie, D., O'Nions, R.K., 1991. Partial melt distributions from inversion of rare earth element concentrations. *Journal of Petrology* 32, 1021–1091.
- McKenzie, D., O'Nions, R.K., 1998. Melt production beneath oceanic islands. *Physics of the Earth and Planetary Interiors* 107, 143–182.
- McMillan, N.J., 1998. Temporal and spatial magmatic evolution of the Rio Grande rift: New Mexico. *Geological Society Guidebook*, 49th Field Conference, pp. 107–116.
- McMillan, N.J., Dickin, A.P., Haag, D., 2000. Evolution of magma source regions in the Rio Grande rift, southern New Mexico. *Geological Society of America Bulletin* 112, 1582–1593.
- McMillan, N.J., Dungan, M.A., 1986. Magma mixing as a petrogenetic process in the development of the Taos Plateau Volcanic Field, New Mexico. *Journal of Geophysical Research* 91, 6029–6045.
- Menzies, M.A., 1989. Cratonic, circumcratonic, and oceanic mantle domains beneath the western United States. *Journal of Geophysical Research* 94, 7899–7915.
- Menzies, M.A., 1990. Archaean, proterozoic, and phanerozoic lithospheres. In: Menzies, M. (Ed.), *Continental Mantle*. Oxford University Press, pp. 67–82.

- Menzies, M.A., Kyle, P.R., 1990. Continental volcanism: a crust mantle probe. In: Menzies, M. (Ed.), *Continental Mantle*. Oxford University Press, pp. 157–177.
- Menzies, M.A., Leeman, W.P., Hawkesworth, C.J., 1983. Isotope geochemistry of Cenozoic volcanic rocks reveals mantle heterogeneity below western USA. *Nature* 303, 205–209.
- Menzies, M.A., Kempton, P.D., Dungan, M.A., 1985. Interaction of continental lithosphere and asthenospheric melts below the Geronimo Volcanic Field, Arizona, U.S.A. *Journal of Petrology* 26, 663–693.
- Menzies, M.A., Kyle, P.R., Jones, M., Ingram, G., 1991. Enriched and depleted source components for tholeiitic and alkaline lavas from Zuni–Bandera, New Mexico: inferences about intraplate processes and stratified lithosphere. *Journal of Geophysical Research* 96, 13 645–13 671.
- Nakamura, N., 1974. Determination of REE, Ba, Mg, Na and K in carbonaceous and ordinary chondrites. *Geochimica et Cosmochimica Acta* 38, 757–775.
- Ormerod, D.S., Hawkesworth, C.J., Rogers, N.W., Leeman, W.P., Menzies, M.A., 1988. Tectonic and magmatic transitions in the Western Great Basin, USA. *Nature* 333, 349–353.
- Perry, F.V., Baldrige, W.S., DePaolo, D.J., 1987. Role of asthenosphere and lithosphere in the genesis of late Cenozoic basaltic rocks from the Rio Grande rift and adjacent regions of the southwestern United States. *Journal Geophysical Research* 92, 9193–9213.
- Perry, F.V., Baldrige, W.S., DePaolo, D.J., 1988. Chemical and isotopic evidence for lithospheric thinning beneath the Rio Grande rift. *Nature* 332, 432–434.
- Reisberg, L., Zindler, A., Marcantonio, F., White, W., Wyman, D., Weaver, B., 1993. Os isotope systematics in ocean island basalts. *Earth and Planetary Science Letters* 120, 149–167.
- Roden, M.R., Smith, D., Murthy, V.R., 1990. Chemical constraints on lithosphere composition and evolution beneath the Colorado Plateau. *Journal of Geophysical Research* 95, 2811–2831.
- Seth, B., Thirlwall, M.F., Houghton, S.L., 2003. Accurate measurements of Th–U isotope ratios for carbonate geochronology using MC-ICP-MS. *Journal of Analytical Atomic Spectrometry* 18, 1323–1330.
- Shaw, J.E., Baker, J.A., Menzies, M.A., Thirlwall, M.F., Ibrahim, K.M., 2003. Petrogenesis of the largest intraplate volcanic field on the Arabian Plate (Jordan): a mixed lithosphere–asthenosphere source activated by lithospheric extension. *Journal of Petrology* 44, 1657–1679.
- Spence, W., Gross, R.S., 1990. A tomographic glimpse of the upper mantle source of magmas of the Jemez lineament, New Mexico. *Journal of Geophysical Research* 95, 10,829–10,849.
- Stormer Jr., J.C., Nicholls, J., 1978. XLFRAC: a program for the interactive testing of magmatic differentiation models. *Computers & Geosciences* 4, 143–159.
- Sun, S., McDonough, W.F., 1989. Chemical and isotope systematics of oceanic basalts: implications for mantle composition and processes. In: Saunders, A.D., Norry, M.J. (Eds.), *Magmatism in the Ocean Basins*. Special Publications, 42. Geological Society, London, pp. 313–345.
- Takahashi, E., Kushiro, I., 1983. Melting of a dry peridotite at high pressures and basalt magma genesis. *American Mineralogist* 68, 859–879.
- Thirlwall, M.F., 1982. A triple-filament method for rapid and precise analysis of rare-earth elements by isotope dilution. *Chemical Geology* 35, 155–166.
- Thirlwall, M.F., 1991a. High precision multicollector isotope analysis of low levels of Nd as oxide. *Chemical Geology* 94, 13–22.
- Thirlwall, M.F., 1991b. Long-term reproducibility of multicollector Sr and Nd isotope ratio analysis. *Chemical Geology* 94, 85–104.
- Thirlwall, M.F., Upton, B.G.J., Jenkins, C., 1994. Interaction between continental lithosphere and the Iceland plume–Sr–Nd–Pb isotope geochemistry of Tertiary basalts, NE Greenland. *Journal of Petrology* 35, 839–879.
- Thirlwall, M.F., Jenkins, C., Vroon, P.Z., Matthey, D.P., 1997. Crustal interaction during construction of ocean islands: Pb–Sr–Nd–O isotope stratigraphy of the shield basalts of Gran Canaria. *Chemical Geology* 135, 233–262.
- Thompson, R.N., Ottley, C.J., Smith, P.M., Pearson, D.G., Dickin, A.P., Morrison, M.A., Leat, P.T., Gibson, S.A., 2005. Source of the Quaternary alkalic basalts, picrites and basanites of the Potrillo Volcanic Field, New Mexico, USA: lithosphere or convecting mantle? *Journal of Petrology* 46, 1603–1643.
- Wang, K., Plank, T., Walker, J.D., Smith, E.I., 2002. A mantle melting profile across the Basin and Range, SW USA. *Journal of Geophysical Research* 107. doi:10.1029/2001JB000209.
- Wendlandt, E., DePaolo, D.J., Baldrige, W.S., 1993. Nd and Sr isotope chronostratigraphy of Colorado Plateau lithosphere: implications for magmatic and tectonic underplating of the continental crust. *Earth and Planetary Science Letters* 116, 23–43.
- West, M., Ni, J., Baldrige, W.S., Wilson, D., Aster, R., Gao, W., Grand, S., 2004. Crust and upper mantle shear wave structure of the southwest United States: implications for rifting and support for high elevation. *Journal of Geophysical Research* 109, B03309. doi:10.1029/2003JB002575.
- Wolff, J.A., Rowe, M.C., Teasdale, R., Gardener, J.N., Ramos, F.C., Heikoop, C.E., 2005. Petrogenesis of Pre-caldera mafic lavas, Jemez Mountains Volcanic Field (New Mexico, USA). *Journal of Petrology* 46, 407–439.
- Workman, R.K., Hart, S.R., 2005. Major and trace element composition of the depleted MORB mantle (DMM). *Earth and Planetary Science Letters* 231, 53–72.